An integral equation method for numerical computation of scattering resonances in a narrow metallic slit

Junshan Lin * and Hai Zhang[†]

Abstract

In this paper we present an efficient and accurate integral equation method to compute the scattering resonances for a subwavelength metallic slit structure. A new boundary integral equation is derived for the scattering problem, and the computation of scattering resonances is reduced to solving the eigenvalues of the corresponding homogeneous formulation over the complex plane. The integral operators are evaluated with high-order precisions by accurate calculations of the Green's functions for the layered medium and accelerated computation of the slit Green's function. The Newton's method is employed for solving the eigenvalues of the boundary integral formulation. We propose an effective strategy for obtaining the initial guesses of scattering resonances by introducing an approximate model for the scattering problem, for which the leading orders of the resonances are derived by asymptotic analysis. Numerical experiments are provided to demonstrate the accuracy, efficiency, and robustness of the method.

Keywords: Integral equation, Helmholtz equation, scattering resonances, subwavelength structure.

1 Introduction

Electromagnetic scattering by subwavelength metallic structures such as apertures and holes has drawn increasing interest since the seminar paper by T. Ebbessen on the so-called extraordinary optical transmission (EOT) and locally field enhancement (LFE) phenomena [11]. The original EOT experiment has triggered tremendous development of subwavelength metallic structures due to their important applications in biological and chemical sensing, near-field spectroscopy, and design of novel optical devices [1, 9, 12, 30].
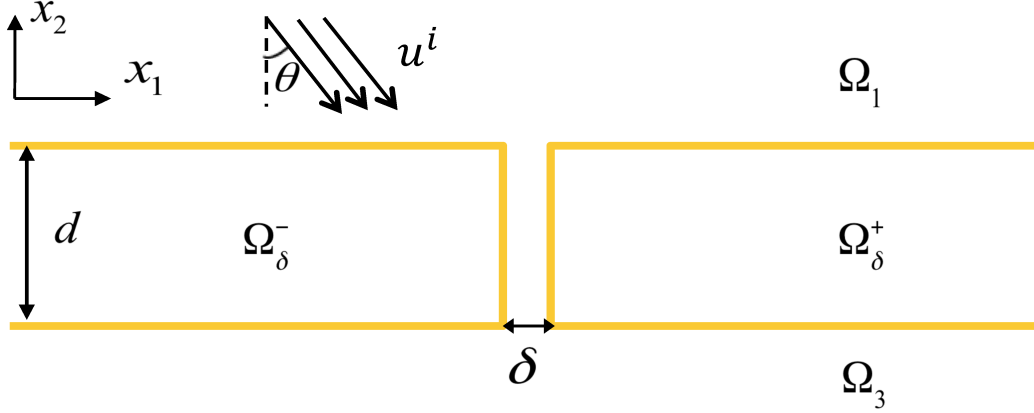
Figure 1: Geometry of the slit model. The domain above the metallic slab, the domain of the metallic slab and the domain below the metallic slab are denoted by Ω_1, Ω_2 and Ω_3 respectively. The slit S_δ perforated in the slab Ω_2 has a rectangular shape of length d and width δ. The remaining part of the metal consists of two disjoint semi-infinite domains Ω_δ^- and Ω_δ^+. The scaling of the geometry is given by $\delta \ll d \sim \lambda$.

For a single subwavelength slit and a periodic array of slits perforated in a perfectly electric conducting (PEC) slab, recently we have presented quantitative analysis of the EOT and LFE phenomena in a series of papers [15, 16, 17, 18, 19]. This provides a complete picture for the enhancement mechanisms in perfect conducting slit structures. A closely related problem of scattering by subwavelength cavities is also investigated in [6, 7]. The main field enhancement mechanism for such subwavelength structures is attributed to the scattering resonances, which are the poles of the resolvent associated with the scattering operator when continued meromorphically to the whole complex plane. If the frequency of the incident wave is close the real part of the resonance (resonance frequency), an enhancement of scattering field is expected if the imaginary part of the resonance is small. The readers are also referred to [3, 4, 5] for recent mathematical studies of several other subwavelength resonators and their resonant scattering phenomena.

In this paper, we investigate numerically the scattering resonances for the more challenging case of real metallic structures, where the metallic slab is not perfectly conducting anymore. The theoretical analysis will be presented in a followup paper [20]. Compared to the PEC case studied previously, optical light can penetrate into real metals with the order of skin depth. Meanwhile, surface plasmon resonances would occur for real metals. In terms of mathematical complications, the former leads to the scattering problem in a layered medium, and the latter gives rise to certain essential scattering poles in the solution formulations. Furthermore, the significant difference in the length scales of the metallic structure proposes additional computational challenges. The hole apertures are usually much smaller than the thickness of the slab, which is comparable to the incident wavelength. In this paper, we investigate the two-dimensional slit structure described in what follows.

The slit is perforated in a metallic slab and the geometry of its cross section is depicted in Figure 1. The metallic slab occupies the domain $\Omega_2 := \{(x_1, x_2) \mid 0 < x_2 < d\}$ on the $x_1 x_2$ plane, and the slit, which is invariant along the x_3 direction, has a rectangular cross section $S_\delta := \{(x_1, x_2) \mid 0 < x_1 < \delta, 0 < x_2 < d\}$. We denote the domain for the remaining

2

part of the metal by Ω_δ, which consists of two disjoint semi-infinite domains Ω_δ^- and Ω_δ^+. Let $\partial\Omega_\delta$ be its boundary and ν be the unit outward normal pointing to the exterior domain. We are interested the subwavelength structure where the slit aperture is narrow compared to the thickness of the slab d and the wavelength of the incident field λ. Let us denote by Ω_1, Ω_3 the semi-infinite domain above and below the slab respectively. Then the relative permittivity ε on the $x_1 x_2$ plane is given by

$$\varepsilon(x) = \begin{cases} \varepsilon_0 & x \in \Omega_1 \cup \Omega_3, \\ \varepsilon_1 & x \in S_\delta, \\ \varepsilon_m & x \in \Omega_\delta, \end{cases}$$

where ε_0, ε_1, and ε_m denote the relative permittivity in the vacuum, in the narrow slit, and in the metal respectively. For simplicity of exposition, we shall assume that $\varepsilon_0 = \varepsilon_1 = 1$. However, the numerical approach presented in this paper can be easily modified for the case when the slit is filled with some dielectric material such that $\varepsilon_1 \neq 1$ [9]. The permittivity of the metal $\varepsilon_m = \varepsilon_m' + i\,\varepsilon_m''$ is a complex number with negative real part ε_m', and it holds that $|\varepsilon_m'| \gg |\varepsilon_m''|$ [26].

We consider the scattering when a polarized time-harmonic electromagnetic wave impinges upon the subwavelength structure. The transverse magnetic (TM) case is considered here by assuming that the incident magnetic field $H^i = (0, 0, u^i)$, where $u^i = e^{ik(d_1 x_1 - d_2(x_2 - d))}$ is a plane wave, k is the wavenumber and $\mathbf{d} = (d_1, -d_2)$ is the direction of incidence with $d_2 > 0$. The total field u after the scattering satisfies the following equations:

$$\begin{cases} \nabla \cdot \left(\dfrac{1}{\varepsilon(x)} \nabla u \right) + k^2 u = 0 & \text{in } \mathbb{R}^2 \backslash \partial\Omega_\delta, \\[2mm] [u] = 0, \ \left[\dfrac{1}{\varepsilon} \dfrac{\partial u}{\partial \nu} \right] = 0 & \text{on } \partial\Omega_\delta, \end{cases} \tag{1.1}$$

where $[\cdot]$ denotes the jump of the quantity when the limit is taken along the positive and negative unit normal direction ν respectively.

Remark *By the scaling invariance of the scattering model, without loss of generality, we shall assume the metal thickness $d = 1$ throughout the paper.*

Due to the smallness of the slit apertures and the presence of the slit corners, the discretization methods based on finite element or finite difference are typically too expensive when applied to solve for the resonances of the scattering problem (1.1). Furthermore, when the infinite exterior domain is truncated into a finite one using an absorbing boundary condition or perfectly matched layer (PML) technique, additional numerical errors will be induced, especially from the reflections near the layer interfaces. Recently, efficient vertical mode matching methods have been developed to compute the optical scattering by subwavelength metallic structures [14, 21, 22]. However, they can not be directly applied to compute the resonances, since the condition number for the discretized linear system is usually very large. In this paper, we propose an efficient and accurate boundary integral-equation method

3

to compute the resonances of the scattering problem (1.1). The integral equation formulation leads to an eigenvalue problem over the complex plane, which is solved by the Newton's method [24, 29]. The proposed numerical approach consists of two main ingredients:

(i) A new boundary integral formulation is derived, which only consists of Neumann data along the slit boundary as unknowns. In addition, fast and high-order evaluations of the integral operators are achieved via accurate calculation of the Green's functions for the layered medium over the tiny slit apertures and accelerated computation of the Green's function for the slit.

(ii) In order to compute the resonances by the Newton's method in an efficient and robust manner, an effective strategy for obtaining the initial guesses of the resonances is developed. This is achieved by introducing an approximate model for the scattering problem (1.1) and deriving the leading orders of the corresponding resonances.

The rest of the paper is organized as follows. We derive the boundary integral equation in Section 2. Its efficient and accurate discretization is elaborated in Section 3. The strategy for obtaining initial guesses of the resonances is presented Section 4, and we demonstrate the performance of the computational approach through various numerical examples in Section 5. Finally, we discuss briefly on the extension of the computational framework to the perfectly conducting slit in Section 6.

2 Integral equation formulation

2.1 Green's functions

Let $G_\ell(x, y)$ be the Green's function for the layered medium such that

$$\Delta_x G_\ell(x, y) + k^2 \varepsilon(x) G_\ell(x, y) = \tilde{\delta}(x - y), \quad x \in \bigcup_{j=1}^{3} \Omega_j, y \in \Omega_\ell, \tag{2.1}$$

$$[G_\ell(x, y)] = \left[\frac{1}{\varepsilon} \frac{\partial G_\ell(x, y)}{\partial x_2} \right] = 0 \quad x_2 = 0, x_2 = 1.$$

Here $\tilde{\delta}$ denotes the Dirac delta function. It can be shown that (see Appendix A)

$$G_1(x, y) = \begin{cases} -\dfrac{i}{4} \left(H_0^{(1)}(k|x - y|) + \dfrac{\varepsilon_m - 1}{\varepsilon_m + 1} H_0^{(1)}(k|x' - y|) \right) + g_{11}(x, y), & x \in \Omega_1, \\[2ex] -\dfrac{i\varepsilon_m}{2(\varepsilon_m + 1)} H_0^{(1)}(k|x - y|) + g_{12}(x, y), & x \in \Omega_2, \\[2ex] g_{13}(x, y), & x \in \Omega_3, \end{cases} \tag{2.2}$$

and

$$
G_2(x,y) = \begin{cases}
-\dfrac{i}{2(\varepsilon_m+1)}H_0^{(1)}(k_m|x-y|) + g_{21}(x,y) \quad x \in \Omega_1, & x \in \Omega_1, \\[3mm]
-\dfrac{i}{4}\left(H_0^{(1)}(k_m|x-y|) + \dfrac{1-\varepsilon_m}{1+\varepsilon_m}H_0^{(1)}(k_m|x'-y|) + \dfrac{1-\varepsilon_m}{1+\varepsilon_m}H_0^{(1)}(k_m|x''-y|)\right) \\[3mm]
+g_{22}(x,y), & x \in \Omega_2, \\[3mm]
-\dfrac{i}{2(\varepsilon_m+1)}H_0^{(1)}(k_m|x-y|) + g_{23}(x,y), & x \in \Omega_3,
\end{cases}
$$

$$(2.3)$$

where $H_0^{(1)}$ is the first kind Hankel function of order 0, x' and x'' are the reflection of x by $x_2 = 1$ and $x_2 = 0$, respectively. That is, $x' = (x_1, 2-x_2)$ and $x'' = (x_1, -x_2)$. $g_{lj}(x,y)$ are continuously differentiable in $\mathbb{R}^2$ and are defined via the Sommerfeld integrals as given in (A.3) - (A.8). On the other hand, the symmetry of the problem geometry implies that

$$
G_3(x_1, x_2; y_1, y_2) = G_1(x_1, 1-x_2; y_1, 1-y_2). \tag{2.4}
$$

Let $G^s(x,y)$ be the Green's function for the slit domain with the zero Neumann boundary condition such that

$$
\begin{cases}
\Delta G^s(x,y) + k^2 G^s(x,y) = \delta(x-y), & x,y \in S_\delta. \\[3mm]
\dfrac{\partial G^s(x,y)}{\partial \nu_x} = 0 & \text{on } \partial S_\delta.
\end{cases}
$$

Then $G^s(x,y)$ adopts the following eigenfunction expansion:

$$
G^s(x,y) = \sum_{n,p=0}^{\infty} c_{np}\phi_{np}(x)\phi_{np}(y), \tag{2.5}
$$

where $c_{np} = \dfrac{1}{k^2 - (n\pi/\delta)^2 - (p\pi)^2}$, $\phi_{np}(x) = \sqrt{\dfrac{a_{np}}{\delta}}\cos\left(\dfrac{n\pi x_1}{\delta}\right)\cos(p\pi x_2)$, and

$$
a_{np} = \begin{cases}
1 & n = p = 0, \\
2 & n \ge 1, p = 0 \quad \text{or,} \quad n = 0, p \ge 1, \\
4 & n \ge 1, p \ge 1.
\end{cases}
$$

2.2 Integral equation over the slit boundary

We denote by Γ_1 and Γ_2 denote the upper and lower slit aperture respectively, and Γ_3 and Γ_4 the left and right slit wall respectively (cf. Figure 2). Let $\tilde{S}_{ij}$ be the single-layer operator given by

$$
\tilde{S}_{ij}[\varphi](y) = \int_{\Gamma_j} G^s(x,y)\varphi(x)\,ds_x \quad y \in \Gamma_i, \tag{2.6}
$$

5

where $G^s(x, y)$ is the Green's function for the slit geometry given in (2.5). Let the single- and double-layer integral operators S_{ij}^ℓ and K_{ij}^ℓ be given by

$$S_{ij}^\ell[\varphi](y) = \int_{\Gamma_j} \Phi_\ell(x, y)\varphi(x) \, ds_x \quad y \in \Gamma_i, \tag{2.7}$$

$$K_{ij}^\ell[\varphi](y) = \gamma_j \int_{\Gamma_j} \Theta_\ell(x, y)\varphi(x) \, ds_x \quad y \in \Gamma_i. \tag{2.8}$$

Here and in what follows, the constant γ_j is defined by

$$\gamma_j = \begin{cases} 1 & j = 1, 2, \\ \dfrac{1}{\varepsilon_m} & j = 3, 4. \end{cases}$$

We define the kernels $\Phi_\ell(x, y)$ as the extension of the Green's function $G_\ell(x, y)$ to the slit boundary by letting

$$\Phi_\ell(x, y) = \begin{cases} \lim\limits_{\substack{h_1 \to 0 \\ x+h_1\nu \in \Omega_1 \cup \Omega_3}} \lim\limits_{\substack{h_2 \to 0 \\ y+h_2\nu \in \Omega_\ell}} G_\ell(x + h_1\nu, y + h_2\nu), & x, y \in \Gamma_1 \cup \Gamma_2, x \neq y, \\[2em] \lim\limits_{\substack{h \to 0 \\ y+h\nu \in \Omega_\ell}} G_\ell(x, y + h\nu), & x \in \Gamma_3 \cup \Gamma_4, y \in \Gamma_1 \cup \Gamma_2, \\[2em] G_\ell(x, y) & x, y \in \Gamma_3 \cup \Gamma_4, x \neq y. \end{cases}$$

The kernel $\Theta_\ell(x, y)$ is defined in a similar manner and is given by

$$\Theta_\ell(x, y) = \begin{cases} \lim\limits_{\substack{h_1 \to 0 \\ x+h_1\nu \in \Omega_1 \cup \Omega_3}} \lim\limits_{\substack{h_2 \to 0 \\ y+h_2\nu \in \Omega_\ell}} \nu_x \cdot \nabla_x G_\ell(x + h_1\nu, y + h_2\nu), & x, y \in \Gamma_1 \cup \Gamma_2, x \neq y, \\[2em] \lim\limits_{\substack{h \to 0 \\ y+h\nu \in \Omega_\ell}} \dfrac{\partial G_\ell(x, y + h\nu)}{\partial \nu_x}, & x \in \Gamma_3 \cup \Gamma_4, y \in \Gamma_1 \cup \Gamma_2, \\[2em] \dfrac{\partial G_\ell(x, y)}{\partial \nu_x} & x, y \in \Gamma_3 \cup \Gamma_4, x \neq y. \end{cases}$$

From the expressions of the Green's function (2.2) and (2.4) and the interface conditions along $x_2 = 0$ and $x_2 = 1$, the kernels $\Phi_\ell(x, y)$ and $\Theta_\ell(x, y)$ are well-defined for $\ell = 1, 2, 3$.

Let u^{ref} be the reference wave field when u^i impinges on the slab structure without the slit ($\delta = 0$). Then it can be calculated that

$$u^{ref}(x) = \begin{cases} u^i(x) + R\, e^{i(\xi x_1 + \rho_0(\xi)(x_2-1))} & x \in \Omega_1 \\[1em] T_1\, e^{i(\xi x_1 + \rho_m(\xi) x_2)} + T_2\, e^{i(\xi x_1 - \rho_m(\xi)(x_2-1))} & x \in \Omega_2, \\[1em] T_3\, e^{i(\xi x_1 - \rho_0(\xi) x_2)} & x \in \Omega_3, \end{cases} \tag{2.9}$$

where

$$\xi = k d_1, \quad \rho_0(\xi) = \sqrt{k^2 - \xi^2}, \quad \rho_m(\xi) = \sqrt{k^2 \varepsilon_m - \xi^2},$$
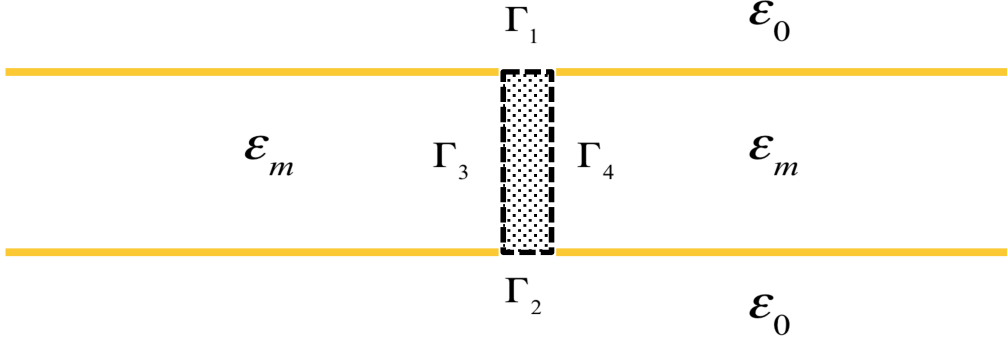$$q(\xi) = (\rho_0(\xi)\varepsilon_m - \rho_m(\xi))^2\, e^{i2\rho_m} - (\rho_0(\xi)\varepsilon_m + \rho_m(\xi))^2.$$

Figure 2: The boundary of the slit ∂S_δ consists of Γ_1 and Γ_2 (slit apertures), and Γ_3 and Γ_4 (slit walls).

The reflection and transmission coefficients are give by

$$R = \frac{1}{q} \cdot \left[\left(\rho_0 \varepsilon_m^2 - \rho_m^2 \right) e^{i2\rho_m} + \left(\rho_m^2 - \rho_0^2 \varepsilon_m^2 \right) \right], \tag{2.10}$$

$$T_1 = -\frac{2}{q} \cdot \varepsilon_m \rho_0 \left(\rho_m - \rho_0 \varepsilon_m \right) e^{i\rho_m}, \tag{2.11}$$

$$T_2 = -\frac{2}{q} \cdot \varepsilon_m \rho_0 \left(\rho_m + \rho_0 \varepsilon_m \right) e^{i\rho_m}, \tag{2.12}$$

$$T_3 = -\frac{4}{q} \cdot \varepsilon_m \rho_0 \rho_m e^{i\rho_m}. \tag{2.13}$$

Let $u^s := u - u^{ref}$ be the scattered field induced by the slit. For convenience of notation, we denote the scattered field and its normal derivative along the slit boundary Γ_j as

$$\varphi_j = u^s|_{\Gamma_j} \quad \text{and} \quad \psi_j = \gamma_j \left. \frac{\partial u^s}{\partial \nu} \right|_{\Gamma_j} \quad (j = 1, 2, 3, 4). \tag{2.14}$$

We also introduce the vector functions $\boldsymbol{\varphi}$ and $\boldsymbol{\psi}$ by letting

$$\boldsymbol{\varphi} = [\varphi_1, \varphi_2, \varphi_3, \varphi_4]^T \quad \text{and} \quad \boldsymbol{\psi} = [\psi_1, \psi_2, \psi_3, \psi_4]^T. \tag{2.15}$$

For $y \in \Omega_\ell \backslash S_\delta$, an application of the Green's second theorem yields (see Appendix B)

$$\beta_\ell u^s(y) = \sum_{j=1}^4 \int_{\Gamma_j} G_\ell(x, y) \left(\gamma_j \frac{\partial u^s(x)}{\partial \nu_x} \right) - \left(\gamma_j \frac{\partial G_\ell(x, y)}{\partial \nu_x} \right) u^s(x) \, ds_x. \tag{2.16}$$

In the above, the coefficient β_ℓ is given by

$$\beta_\ell = \begin{cases} 1 & \ell = 1, 3, \\ \dfrac{1}{\varepsilon_m} & \ell = 2. \end{cases}$$

7

By taking the limit of (2.16) with $\ell = 1$ to the slit boundary Γ_1 and using the jump condition for the double layer potential, it is seen that for $y \in \Gamma_1$,

$$\frac{\varepsilon_m}{\varepsilon_m + 1}\varphi_1 + K_{11}^1[\varphi_1] + K_{12}^1[\varphi_2] + K_{13}^1[\varphi_3] + K_{14}^1[\varphi_4] = S_{11}^1[\psi_1] + S_{12}^1[\psi_2] + S_{13}^1[\psi_3] + S_{14}^1[\psi_4]. \quad (2.17)$$

Similarly, for $y \in \Gamma_2$, it follows that

$$\frac{\varepsilon_m}{\varepsilon_m + 1}\varphi_2 + K_{21}^3[\varphi_1] + K_{22}^3[\varphi_2] + K_{23}^3[\varphi_3] + K_{24}^3[\varphi_4] = S_{21}^3[\psi_2] + S_{22}^3[\psi_2] + S_{23}^3[\psi_3] + S_{24}^3[\psi_4]. \quad (2.18)$$

Taking the limit of (2.16) with $\ell = 2$ to the slit boundary Γ_3 and Γ_4 respectively, we obtain the following two integral equations

$$\frac{1}{2\varepsilon_m}\varphi_3 + K_{31}^2[\varphi_1] + K_{32}^2[\varphi_2] + K_{33}^2[\varphi_3] + K_{34}^2[\varphi_4] = S_{31}^2[\psi_3] + S_{32}^2[\psi_2] + S_{33}^2[\psi_3] + S_{34}^2[\psi_4],$$
$$(2.19)$$

$$\frac{1}{2\varepsilon_m}\varphi_4 + K_{41}^2[\varphi_1] + K_{42}^2[\varphi_2] + K_{43}^2[\varphi_3] + K_{44}^2[\varphi_4] = S_{41}^2[\psi_4] + S_{42}^2[\psi_2] + S_{43}^2[\psi_3] + S_{44}^2[\psi_4].$$
$$(2.20)$$

Define the multiplication operator

$$\mathbb{D} = \begin{bmatrix} \frac{\varepsilon_m}{\varepsilon_m+1}I_1 & 0 & 0 & 0 \\ 0 & \frac{\varepsilon_m}{\varepsilon_m+1}I_2 & 0 & 0 \\ 0 & 0 & \frac{1}{2\varepsilon_m}I_3 & 0 \\ 0 & 0 & 0 & \frac{1}{2\varepsilon_m}I_4 \end{bmatrix},$$

where $I_j : L^2(\Gamma_j) \to L^2(\Gamma_j)$ are identity operators. Let

$$\mathbb{K}^e = \begin{bmatrix} K_{11}^1 & K_{12}^1 & K_{13}^1 & K_{14}^1 \\ K_{21}^3 & K_{22}^3 & K_{23}^3 & K_{24}^3 \\ K_{31}^2 & K_{32}^2 & K_{33}^2 & K_{34}^2 \\ K_{41}^2 & K_{42}^2 & K_{43}^2 & K_{44}^2 \end{bmatrix} \quad \text{and} \quad \mathbb{S}^e = \begin{bmatrix} S_{11}^1 & S_{12}^1 & S_{13}^1 & S_{14}^1 \\ S_{21}^3 & S_{22}^3 & S_{23}^3 & S_{24}^3 \\ S_{31}^2 & S_{32}^2 & S_{33}^2 & S_{34}^2 \\ S_{41}^2 & S_{42}^2 & S_{43}^2 & S_{44}^2 \end{bmatrix},$$

Then we can write the system of the integral equations (2.17)- (2.20) as the following concise form

$$(\mathbb{D} + \mathbb{K}^e)[\boldsymbol{\varphi}] = \mathbb{S}^e[\boldsymbol{\psi}], \quad (2.21)$$

where the vector functions $\boldsymbol{\varphi}$ and $\boldsymbol{\psi}$ are Dirichlet and Neumann data on the slit boundary defined in (2.15).

Inside the slit S_δ, using the Green's function (2.5) with the zero Neumann boundary condition, it follows that the total field u can be expressed as

$$u(y) = \int_{\partial S_\delta} G^s(x, y)\frac{\partial u(x)}{\partial \nu} ds_x \quad \text{for } y \in S_\delta.$$

The continuity of the single layer potential yields

$$u(y) = \sum_{j=1}^{4} \int_{\Gamma_j} G^s(x, y) \frac{\partial u(x)}{\partial \nu} \, ds_x, \quad y \in \Gamma_i, i = 1, 2, 3, 4. \tag{2.22}$$

Using the relation $u = u^s + u^{ref}$, we express the above integral equation in the operator form as

$$\boldsymbol{\varphi} = -\mathbb{S}^i[\boldsymbol{\psi}] + \mathbf{f}, \tag{2.23}$$

where the operator

$$\mathbb{S}^i = \begin{bmatrix} \tilde{S}_{11} & \tilde{S}_{12} & \tilde{S}_{13} & \tilde{S}_{14} \\ \tilde{S}_{21} & \tilde{S}_{22} & \tilde{S}_{23} & \tilde{S}_{24} \\ \tilde{S}_{31} & \tilde{S}_{32} & \tilde{S}_{33} & \tilde{S}_{34} \\ \tilde{S}_{41} & \tilde{S}_{42} & \tilde{S}_{43} & \tilde{S}_{44} \end{bmatrix} \quad \text{and} \quad \mathbf{f} = u^{ref}\big|_{\partial S_\delta} + \mathbb{S}^i \left[\partial_\nu u^{ref}\big|_{\partial S_\delta} \right].$$

By combining (2.21) and (2.23), one may eliminate $\boldsymbol{\varphi}$ and obtain the following integral equation for the scattering problem (1.1):

$$\left(\mathbb{S}^{(e)}(k) + (\mathbb{D}(k) + \mathbb{K}^{(e)}(k)) \mathbb{S}^{(i)}(k) \right) \boldsymbol{\psi} = (\mathbb{D}(k) + \mathbb{K}^{(e)}(k))\mathbf{f}. \tag{2.24}$$

Here we express explicitly the dependence of the operators on k. Once the Neumann data $\boldsymbol{\psi}$ is computed, the Dirichlet data $\boldsymbol{\varphi}$ can be evaluated via the integral equation (2.23).

A scattering resonance of (1.1) is defined as a complex number k such that there exists a nontrivial solution when the incident field is zero. This corresponds to the characteristic values of the operator-valued function $\mathbb{S}^{(e)} + (\mathbb{D} + \mathbb{K}^{(e)}) \mathbb{S}^{(i)}$ with respect to the variable k. Namely, we solve for k over the complex plane such that the homogeneous equation

$$\left(\mathbb{S}^{(e)}(k) + (\mathbb{D}(k) + \mathbb{K}^{(e)}(k)) \mathbb{S}^{(i)}(k) \right) \boldsymbol{\psi} = 0 \tag{2.25}$$

attains nontrivial solution.

To solve the above eigenvalue problem, we employ the Newton's method as described in [24, 29]. The method start from some initial guess for the eigenvalue and eigenvectors, and update the solution iteratively. This requires the discretization of the corresponding integral operators and an effective strategy for choosing initial-guess values, which are discussed in Section 3 and 4 respectively.

3   Numerical computation of the integral operators

3.1   Numerical evaluation of the Green's function for layered medium

The evaluation of the kernels $\Phi_\ell(x, y)$ and $\Theta_\ell(x, y)$, or equivalently G_ℓ and their derivatives, involves the computation of functions $g_{lj}(x, y)$, which are defined via the Sommerfeld integrals (A.3) - (A.8). We adopt a contour integration approach together with the smooth-windowing

technique as introduced in [27, 28]. An improved discretization strategy is proposed in what follows by treating the slow-varying integral and the oscillatory integral separately. The new strategy leads to a higher-order accuracy compared to the original version in [27, 28], especially for tiny slit apertures with size δ. In addition, the presence of plasmonic resonance poles induced by the metal involves new complexities which need to be addressed separately.
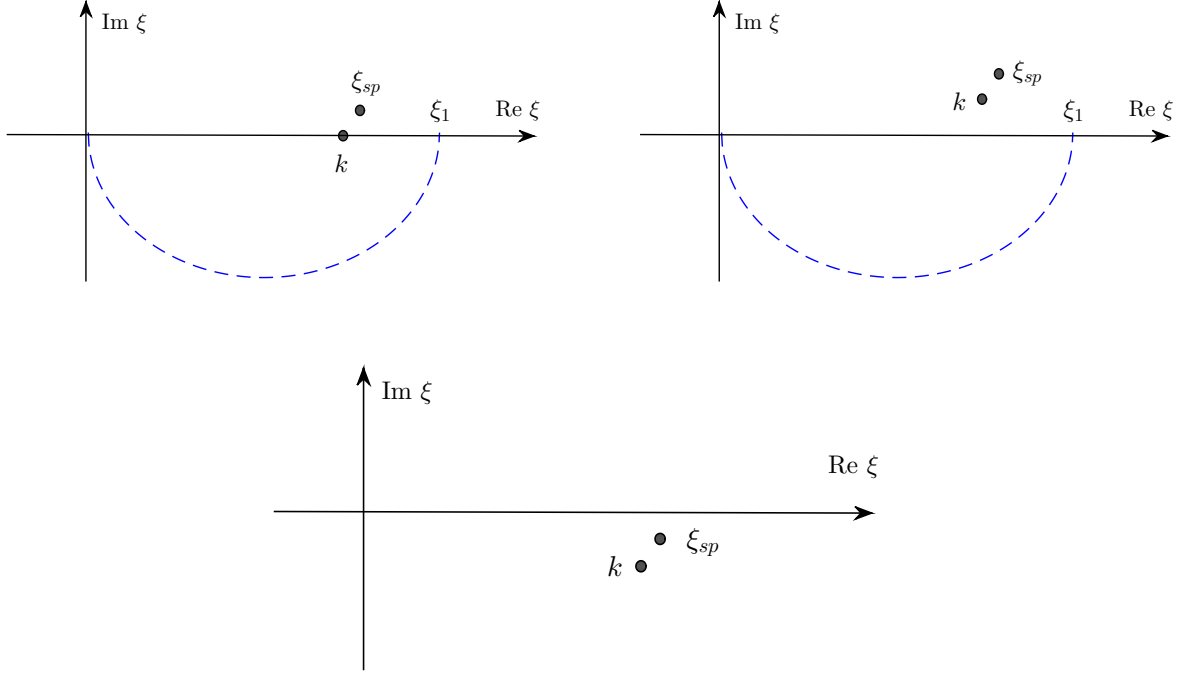

Figure 3: ξ_{sp} for given complex-valued k.

For clarity we elaborate on the computation of $g_{11}(x, y)$, and the others are treated similarly. To this end, one needs to compute the Sommerfeld integrals

$$\bar{I} := \int_0^\infty h(\xi) \, d\xi = \int_0^\infty \frac{\rho_0(\xi)\varepsilon_m + \rho_m(\xi)}{\rho_0(\xi) \cdot (\rho_o(\xi) + \rho_m(\xi)) \cdot q(\xi)} e^{i\rho_0(x_2+y_2-2)} \cos(\xi(x_1 - y_1)) \, d\xi$$

and

$$\tilde{I} := \int_0^\infty \tilde{h}(\xi) \, d\xi = \int_0^\infty \frac{p(\xi)e^{i2\rho_m}}{\rho_0(\xi) \cdot q(\xi)} e^{i\rho_0(x_2+y_2-2)} \cos(\xi(x_1 - y_1)) \, d\xi,$$

where

$$\rho_0(\xi) = \sqrt{k^2 - \xi^2}, \quad \rho_m(\xi) = \sqrt{k^2\varepsilon_m - \xi^2},$$
$$p(\xi) = (\varepsilon_m + 1)\left(\rho_0(\xi)^2\varepsilon_m^2 - \rho_m(\xi)^2\right) - (\varepsilon_m - 1)\left(\rho_0(\xi)\varepsilon_m - \rho_m(\xi)\right)^2,$$
$$q(\xi) = \left(\rho_0(\xi)\varepsilon_m - \rho_m(\xi)\right)^2 e^{i2\rho_m} - \left(\rho_0(\xi)\varepsilon_m + \rho_m(\xi)\right)^2.$$

Here and henceforth, the function $f(z) = \sqrt{z}$ is understood as an analytic function defined in the domain $\mathbf{C}\backslash\{-it : t \geq 0\}$ by

$$z^{\frac{1}{2}} = |z|^{\frac{1}{2}} e^{\frac{1}{2}i \arg z}.$$

10

Let us focus on the first integral. Note that $\rho_o(\xi) + \rho_m(\xi) \neq 0$ and the integrand attains poles for ξ satisfying

$$\rho_0(\xi) = 0 \quad \text{and} \quad q(\xi) = 0.$$

When $k \neq 0$, it is observed that $\xi = \pm k$ are branch points for $\rho_0(\xi)$ and removable singularities for $1/\rho_0(\xi)$. The branch point for $\rho_m(\xi)$ is $\xi = k\sqrt{\varepsilon_m}$, which lies in the first quadrant with large real part by noting that $\varepsilon'_m < 0$ and $|\varepsilon'_m| \gg |\varepsilon''_m|$. The roots of $q(\xi)$ correspond to surface plasmonic resonance frequencies of the metallic slab. More precisely, if one considers the scattering problem (1.1) without the slit such that $\delta = 0$ and no source is present, then from (2.9) - (2.13), we see that non-trivial solutions exist when $q(\xi) = 0$. The roots, which are called surface plasmonic resonance frequencies, lies in the vicinity of

$$\xi_{sp} = k\sqrt{\varepsilon_m/(\varepsilon_m + 1)}.$$

They are essential singularities for $1/q(\xi)$. Note that $\varepsilon'_m < -1$ and $|\varepsilon'_m| \gg |\varepsilon''_m|$, hence it holds that $|\xi_{sp}| > |k|$. The relative positions of k and ξ_{sp} are shown in Figure 3.

The whole integral $\bar{I}$ is decomposed into three parts as follows:

$$\bar{I} = \bar{I}_1 + \bar{I}_2 + \bar{I}_3$$
$$= \int_0^{\xi_1} h(\xi)\, d\xi + \int_{\xi_1}^{\xi_2} h(\xi)\, d\xi + \int_{\xi_2}^{\infty} h(\xi)\, d\xi.$$

In the above, the real positive number ξ_1 is chosen to be larger than $Re\,\xi_{sp}$ so that the interval $(0, \xi_1)$ contains all possible poles of the integrand. We set

$$\xi_2 = \max\{\xi_1, 2\pi/|x_1 - y_1|\}$$

such that the integrand for I_2 is a slow varying function in the interval (ξ_1, ξ_2), and I_3 is an oscillatory integral. The computation of each part can be accomplished by the following process.

For $\bar{I}_1$, two different approaches are applied for $Im\,k \geq 0$ and $Im\,k < 0$ respectively.

(i) $Im\,k \geq 0$: One chooses a simple curve C in the fourth quadrant that starts at the origin and ends at $\xi = \xi_1$ (see Figure 3). By the Cauchy integral theorem,

$$\bar{I}_1 = \int_C h(\xi)\, d\xi = \int_{-1}^1 h(r(t))\, dt,$$

where $\xi = r(t)$ is the parameterization of the curve C. Due to the smoothness of the integrand over the curve C, $\bar{I}_1$ can be computed with high-oder accuracy by the Clenshaw-Curtis quadrature [8].

(i) $Im\,k < 0$: Due to the presence of the branch point $\xi = k$ and the plasmonic resonances poles near ξ_{sp}, one can not find a closed curve consisting of the interval $(0, \xi_1)$ so that $h(\xi)$ is analytic inside the curve. Instead, observing that $h(\xi)$ is analytic on the subinterval $(0, Re\,k)$ and $(Re\,k, \xi)$ respectively, I_1 is computed directly by evaluating the integral on each subinterval separately. However, when $|Im\,k|$ is small, the

integrand attains large values near the end point $Re\,k$. In order to achieve high-order accuracy, graded meshes are employed to discretize the interval and the Fourier series representation of h is used [10]. Such techniques is also used to discretize the integral operators in Section 3.3.

The integrand for $\bar{I}_2$ is non-oscillatory on (ξ_1, ξ_2). Typically, $|x_1 - y_1|$ is very small due to the smallness of the slit aperture size δ, hence the interval size $A = |\xi_2 - \xi_1|$ is large. By a change of variable $\xi = \xi_1 + A\bar{\xi}$, it follows that

$$\bar{I}_2 = A \int_0^1 h(\xi_1 + A\bar{\xi})d\bar{\xi}.$$

Note that $h(\xi)$ decays as $1/|\xi|^3$ when $|\xi| \to \infty$, which implies that the function value $h(\xi_1 + A\bar{\xi})$ spans from order $O(1)$ to $O(|x_1 - y_1|^3)$ in $(0,1)$. As such the derivate of $h(\xi + A\bar{\xi})$ is extremely large near the left end point, and the Clenshaw-Curtis quadrature will not yield high-order accuracy for computing $\bar{I}_2$. Instead, graded meshes are used again to discretize the interval and a Fourier series expansion of h is adopted.

Finally the evaluation of the oscillatory integral $\bar{I}_3$ is based on the smooth-windowing technique using the partition of the unity [28]. For a given constant $0 < \alpha < 1$, we define a smooth cut-off (window) function

$$\eta_B(\bar{\xi}) = \begin{cases} 1 & |\bar{\xi}| \le \alpha B, \\ e^{\frac{2e^{-1/z}}{z-1}}, & \alpha B < |\bar{\xi}| < B, z = \frac{|\bar{\xi}| - \alpha B}{(1-\alpha)B} \\ 0 & |\bar{\xi}| > B. \end{cases} \tag{3.1}$$

We approximate the integral by multiplying the integrand with the window function:

$$\bar{I}_3 = \xi_2 \int_0^\infty h(\xi_2(1+\bar{\xi}))\, d\bar{\xi} \approx \xi_2 \int_0^B h(\xi_2(1+\bar{\xi})) \cdot \eta_B(\bar{\xi})\, d\bar{\xi}.$$

The integrand is smooth and the Clenshaw-Curtis quadrature is applied.

n	$|\bar{I} - \bar{I}^{(1)}|$	$|\bar{I} - \bar{I}^{(2)}|$
20	3.43×10^{-3}	6.53×10^{-2}
40	1.39×10^{-5}	2.22×10^{-2}
80	3.72×10^{-9}	1.14×10^{-3}

Table 1: The accuracy of numerical integration obtained by treating the slow-varying integral and the oscillatory integral separately, and by applying the Clenshaw-Curtis quadrature directly on the whole integral. n denotes the number of grid points used for each subinterval. The same number of grid points is used to compute $\bar{I}^{(2)}$.

To demonstrate the accuracy of numerical integration, we consider the evaluation of the integral with $k = 0.5$, $|x_1 - y_1| = 0.02$ and $x_2 = y_2 = 1$. The permittivity is set as

12

$\varepsilon_m = -10 + i$. The real integral value $\bar{I} = -0.088734021404942 - 0.122293333722895i$ (up to machine precision). To demonstrate the improved accuracy by treating the slow-varying integral and the oscillatory integral separately, the second column of Table 3.1 shows the accuracy of numerical integration by employing the quadrature rule described above, which we denote as $\bar{I}^{(1)}$. The third column shows the numerical value $\bar{I}^{(2)}$ that is obtained by using the same window function but by applying the Clenshaw-Curtis quadrature directly on the whole integral.

3.2 Accelerated computation of the slit Green's function

The slit Green's function $G^s(x, y)$ adopts the expansion (2.5). However, the expansion series converges slowly with a rate of $O\left(\frac{1}{n^2 + p^2}\right)$ and one also needs to take double sum to evaluate. The convergence rate is even slower when the target point y and the source point x are close. To remedy this issue, we adopt the Kummer's transformation technique to accelerate the evaluation of the Green's function [25]. The idea is to convert the slowly convergent series into two series, where the slower series can be summed analytically and the faster series can be computed accurately by taking the sum with only a smaller number of terms.

We express the slit Green's function as

$$G^s(x, y) = \sum_{n=0}^{\infty} \omega_n \, g_n(x_2, y_2) \, \cos\left(\frac{n\pi x_1}{\delta}\right) \cos\left(\frac{n\pi y_1}{\delta}\right), \tag{3.2}$$

where

$$\omega_n = \begin{cases} 1 & n = 0, \\ 2/\delta & n \geq 1, \end{cases}$$

and $g_n(x_2, y_2)$ is the one-dimensional Green's function that solves

$$g_n''(x_2, y_2) + (k^2 - (n\pi/\delta)^2)g_n(x_2, y_2) = \tilde{\delta}(x_2 - y_2), \quad g_n'(0, y_2) = g_n'(1, y_2) = 0.$$

By a direct calculation, it follows that

$$g_n(x_2, y_2) = -\frac{i}{2a_n} e^{ia_n|x_2 - y_2|} - \frac{i}{2a_n \cdot b_n} \left(e^{ia_n|x_2 + y_2|} + e^{ia_n|2 - x_2 - y_2|} + e^{ia_n|2 - x_2 + y_2|} + e^{ia_n|2 + x_2 - y_2|}\right), \tag{3.3}$$

where

$$a_n = \sqrt{k^2 - (n\pi/\delta)^2} \quad \text{and} \quad b_n = 1 - e^{i2a_n}.$$

It is clear that for $n \gg 1$,

$$a_n = \frac{in\pi}{\delta}\left(1 - \frac{1}{2}\left(\frac{k\delta}{n\pi}\right)^2 + O\left(\frac{k\delta}{n\pi}\right)^4\right) \quad \text{and} \quad b_n = 1 + O\left(e^{-n\pi/\delta}\right). \tag{3.4}$$

Lemma 3.1 *Let $\phi_n(t) = -\frac{i}{2a_n} e^{ia_n t}$, then for $n \gg 1$,*

$$\phi_n(t) = \phi_{n,0}(t) + O\left(\frac{\delta}{n\pi}\right)^3 \quad \text{for } 0 < t \leq 4, \tag{3.5}$$

13

where

$$\phi_{n,0}(t) = -\frac{\delta}{2n\pi}e^{-\frac{n\pi}{\delta}t}. \tag{3.6}$$

Proof. From the asymptotic expansion (3.4), we obtain

$$\phi_n(t) = -\frac{\delta}{2n\pi}\left(1 + \frac{1}{2}\left(\frac{k\delta}{n\pi}\right)^2 + O\left(\frac{k\delta}{n\pi}\right)^4\right) \cdot e^{-\frac{n\pi}{\delta}t} \cdot \left(1 + \frac{1}{2}\frac{k^2\delta}{n\pi}t + O\left(\frac{\delta}{n\pi}\right)^3\right)$$

$$= -\frac{\delta}{2n\pi}e^{-\frac{n\pi}{\delta}t} - \frac{1}{4}\left(\frac{k\delta}{n\pi}\right)^2 te^{-\frac{n\pi}{\delta}t} + O\left(\frac{\delta}{n\pi}\right)^3.$$

Note that for fixed $n > 1$, $te^{-\frac{n\pi}{\delta}t}$ attains the maximum when $t = \frac{\delta}{n\pi}$, hence the assertion follows. $\qquad\square$

We define the singular part of the Green's function by letting

$$G_0^s(x,y) = \sum_{n=1}^{\infty} \omega_n \left[\phi_{n,0}(|x_2 - y_2|) + \phi_{n,0}(|x_2 + y_2|) + \phi_{n,0}(|2 - x_2 - y_2|)\right] \cos\left(\frac{n\pi x_1}{\delta}\right)\cos\left(\frac{n\pi y_1}{\delta}\right), \tag{3.7}$$

where $\phi_{n,0}$ is given by (3.6).

Lemma 3.2 $G_0^s(x,y)$ *can be expressed as*

$$G_0^s(x,y) = \frac{1}{4\pi}\sum_{j=1}^{6}\left[\ln\left(1 - e^{z_j}\right) + \ln\left(1 - e^{\bar{z}_j}\right)\right], \tag{3.8}$$

where

$$z_1 = -\frac{\pi}{\delta}(|x_2 - y_2| + i(x_1 - y_1)), \qquad z_2 = -\frac{\pi}{\delta}(|x_2 - y_2| + i(x_1 + y_1)),$$

$$z_3 = -\frac{\pi}{\delta}(|x_2 + y_2| + i(x_1 - y_1)), \qquad z_4 = -\frac{\pi}{\delta}(|x_2 + y_2| + i(x_1 + y_1)),$$

$$z_5 = -\frac{\pi}{\delta}(|2 - x_2 - y_2| + i(x_1 - y_1)), \qquad z_6 = -\frac{\pi}{\delta}(|2 - x_2 - y_2| + i(x_1 + y_1)),$$

In addition,

$$G^s(x,y) - G_0^s(x,y) = \delta^2 \cdot \sum_{n=0}^{\infty} \tilde{a}_n(x,y), \tag{3.9}$$

where

$$\sup_{x,y}|\tilde{a}_n(x,y)| \sim O\left(\frac{1}{n^3}\right) \quad \text{for } n \gg 1.$$

Remark *To evaluate $G^s(x,y)$, we decompose it as $G_0^s(x,y)$ and $G^s(x,y) - G_0^s(x,y)$. G_0^s is given explicitly in (3.8), and one only needs a small number of terms to evaluate $G^s - G_0^s$.*

Proof. By substituting (3.3) into the expansion (3.2), and using the asymptotic expansion (3.5) with $t = |x_2 - y_2|$, $|x_2 + y_2|$, and $|2 - x_2 - y_2|$ respectively, we obtain

$$G^s(x, y) - G_0^s(x, y) = \sum_{n=0}^{\infty} \hat{a}_n(x, y),$$

where

$$\hat{a}_n(x, y) = \delta \cdot O\left(\frac{\delta}{n\pi}\right)^3 - \frac{i\omega_n}{2a_n \cdot b_n}\left(e^{ia_n|2 - x_2 + y_2|} + e^{ia_n|2 + x_2 - y_2|}\right) \cos\left(\frac{n\pi x_1}{\delta}\right) \cos\left(\frac{n\pi y_1}{\delta}\right)$$

$$= \delta^2 \cdot O\left(\frac{1}{n^3}\right) \quad \text{for } n \gg 1.$$

Hence the assertion (3.9) holds. To show (3.8), by setting $t = |x_2 - y_2|$ we see that

$$\sum_{n=1}^{\infty} \omega_n \, \phi_{n,0}(|x_2 - y_2|) \cos\left(\frac{n\pi x_1}{\delta}\right) \cos\left(\frac{n\pi y_1}{\delta}\right)$$

$$= -\sum_{n=1}^{\infty} \frac{2}{\delta} \cdot \frac{\delta}{2n\pi} e^{-\frac{n\pi}{\delta}|x_2 - y_2|} \cdot \frac{1}{4}\left(e^{\frac{in\pi}{\delta}(x_1 - y_1)} + e^{-\frac{in\pi}{\delta}(x_1 - y_1)} + e^{\frac{in\pi}{\delta}(x_1 + y_1)} + e^{-\frac{in\pi}{\delta}(x_1 + y_1)}\right)$$

$$= -\sum_{n=1}^{\infty} \frac{1}{4n\pi}(e^{nz_1} + e^{n\bar{z}_1} + e^{nz_2} + e^{n\bar{z}_2})$$

$$= \frac{1}{4\pi}\left[\ln\left(1 - e^{z_1}\right) + \ln\left(1 - e^{\bar{z}_1}\right) + \ln\left(1 - e^{z_2}\right) + \ln\left(1 - e^{\bar{z}_2}\right)\right].$$

Similar calculations for $t = |x_2 + y_2|$ and $t = |2 - x_2 - y_2|$ lead to the formula (3.8). □

3.3 Discretization of the integral operators

To discretize the single-layer operators S_{ij}^{ℓ} and $\tilde{S}_{ij}$ and the double-layer integral operators K_{ij}^{ℓ} in (2.25), we parameterize the slit boundary so that $x_1 = \delta\tau$ for $\tau \in (0, 1)$ over the slit apertures Γ_1 and Γ_2, and $x_2 = \tau$ for $\tau \in (0, 1)$ over the slit walls Γ_3 and Γ_4. We express the integral operators S_{ij}^{ℓ}, $\tilde{S}_{ij}$ and K_{ij}^{ℓ} in the following generic forms without distinguishing their expressions on different segments of the slit boundary:

$$\int_0^1 M_{\ell}(\tau, \sigma)\psi(\tau)\,d\tau, \quad \sigma \in (0, 1), \tag{3.10}$$

$$\int_0^1 \hat{M}(\tau, \sigma)\psi(\tau)\,d\tau, \quad \sigma \in (0, 1), \tag{3.11}$$

$$\int_0^1 N_{\ell}(\tau, \sigma)\varphi(\tau)\,d\tau \quad \sigma \in (0, 1). \tag{3.12}$$

In the above, $M_{\ell}(\tau, \sigma)$, $\hat{M}(\tau, \sigma)$ and $N_{\ell}(\tau, \sigma)$ denote the kernels $\Phi_{\ell}(x, y)$, $G^s(x, y)$ and $\Theta_{\ell}(x, y)$ in the (τ, σ)-coordinate, respectively. $\psi(\tau)$ and $\varphi(\tau)$ denote the density functions with the

parameterization. Recall that the Green's function $G_\ell(x, y)$ are given by (2.2) and (2.3), it is clear that if the source point x and the target point y lies in the same line segment, $M_\ell(\tau, \sigma)$ attains the logarithm singularity when $\tau = \sigma$. From (3.8), the kernel $\hat{M}(\tau, \sigma)$ also attains the logarithm singularity when $\tau = \sigma$. On the other hand, by noting the fact that $\partial_{\nu_x} H_0^{(1)}(k|x - y|) = 0$ and $\partial_{\nu_x} H_0^{(1)}(k_m|x - y|) = 0$ if the source point x and the target point y lie in the same line segment, we deduce that the kernel $N_\ell(\tau, \sigma)$ does not contain singularity when $\tau = \sigma$. In what follows, we discuss their numerical discretization in details.

3.3.1 Numerical evaluation of (3.10) and (3.11)

There exist two types of singularities for the integrand of (3.10) and (3.11). One arises from the logarithm singularity of the kernel $M_\ell(\tau, \sigma)$ and $\hat{M}(\tau, \sigma)$ mentioned above, and the other arises from the singularities of the density function $\psi(\tau)$ at the two endpoints of the interval $(0, 1)$. In fact, $\psi(\tau) \in H^{-1/2}(0, 1)$ where $H^{-1/2}(0, 1)$ is the standard fractional Sobolev space [2]. To evaluate the singular integrals accurately, we employ the Nystrom scheme in combination with graded meshes techniques following the procedure described in [10, 23]. In the following, for brevity we only describe the calculation of (3.10) and the evaluation of (3.11) is similar.

For fixed target point $y \in \Gamma_i$, when the source point $x \in \Gamma_j$ with $j = i$, the kernel $M_\ell(\tau, \sigma)$ can be splitted into a singular part and a smooth part as follows:

$$M_\ell(\tau, \sigma) = M_{\ell,1}(\tau, \sigma) \ln\left(4 \sin^2\left(\frac{\sigma - \tau}{2}\right)\right) + M_{\ell,2}(\tau, \sigma),$$

where

$$M_{\ell,1}(\tau, \sigma) = \frac{\alpha_\ell}{4\pi} J_0(k\tilde{\alpha}_\ell |\sigma - \tau|), \quad M_{\ell,2}(\tau, \sigma) = M_\ell(\tau, \sigma) - M_{\ell,1}(\tau, \sigma).$$

with

$$\alpha_\ell = \begin{cases} \frac{2\varepsilon_m}{\varepsilon_m + 1}, & \ell = 1, 3; \\ 1, & \ell = 2. \end{cases} \quad \text{and} \quad \tilde{\alpha}_\ell = \begin{cases} \delta, & \ell = 1, 3; \\ 1, & \ell = 2. \end{cases}$$

It is clear that both $M_{\ell,1}(\tau, \sigma)$ and $M_{\ell,2}(\tau, \sigma)$ are smooth functions on $(0, 1) \times (0, 1)$.

The graded mesh is realized by introducing a change of variable

Figure 4: Graded mesh over the slit boundary.

$$\tau = w(s) := \frac{v(s)^r}{v(s)^r + v(2\pi - s)^r}, \quad 0 < s < 2\pi,$$

where $r \geq 2$ and

$$v(s) = \left(\frac{1}{r} - \frac{1}{2}\right)\left(\frac{\pi - s}{\pi}\right)^3 + \frac{1}{r}\frac{s - \pi}{\pi} + \frac{1}{2}.$$

The function $w(s)$ is smooth and increasing in $(0, 2\pi)$, and it holds that $w^{(i)}(0) = w^{(i)}(2\pi) = 0$ for $i = 0, \cdots, r - 1$. If the grid points $\{s_j\}_{j=0}^{2n}$ are equally distributed on the interval $[0, 2\pi]$,
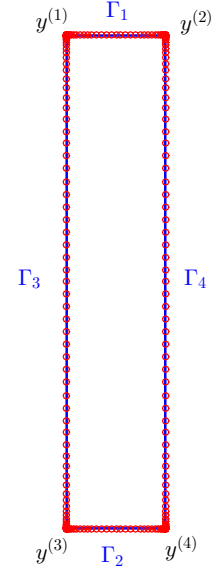
then $\{w(s_j)\}_{j=1}^{2n}$ yields a graded mesh where one half of the grid points is equally distributed over the whole interval $(0, 1)$, and the other half is accumulated towards the end points $\tau = 0$ and $\tau = 1$ (see Figure 4).

With the change of variable, the integral

$$\int_0^1 M_\ell(\tau, \sigma)\psi(\tau)d\tau = \int_0^{2\pi} M_\ell(w(s), w(t))\psi(\tau(s))w'(s)\, ds.$$

Correspondingly, we split the kernel M_ℓ as

$$M_\ell(w(s), w(t)) = \tilde{M}_{\ell,1}(s, t) \ln\left(4\sin^2\left(\frac{t-s}{2}\right)\right) + \tilde{M}_{\ell,2}(s, t),$$

where

$$\tilde{M}_{\ell,1}(s, t) = M_{\ell,1}(w(s), w(t)) \quad\text{and}\quad \tilde{M}_{\ell,2}(s, t) = M_\ell(w(s), w(t)) - M_{\ell,1}(w(s), w(t)).$$

We choose an equidistant set of grid points $s_j = j\pi/n$ for $j = 0, 1, \cdots, 2n - 1$. Using the quadrature rules (cf. [10, 23])

$$\int_0^{2\pi} \ln\left(4\sin^2\left(\frac{t-s}{2}\right)\right) f(s)\, ds \approx \sum_{j=0}^{2n-1} R_j(t)f(s_j), \tag{3.13}$$

where the quadrature weight

$$R_j(t) = -\frac{2\pi}{n}\sum_{m=1}^{n-1}\frac{1}{m}\cos(m(t - t_j)) - \frac{\pi}{n}\cos(n(t - t_j)),$$

and

$$\int_0^{2\pi} f(s)\, ds \approx \frac{\pi}{n}\sum_{j=0}^{2n-1} f(s_j), \tag{3.14}$$

it follows that

$$\int_0^{2\pi} M_\ell(w(s), w(t))\psi(\tau(s))w'(s)\, ds$$

$$\approx \sum_{j=1}^{2n-1} R_j(t)\,\tilde{M}_{\ell,1}(s_j, t)\,\psi(\tau(s_j))\,w'(s_j) + \frac{\pi}{n}\sum_{j=1}^{2n-1}\tilde{M}_{\ell,2}(s_j, t)\,\psi(\tau(s_j))\,w'(s_j). \tag{3.15}$$

When the source point $x \in \Gamma_j$ with $j \neq i$, for sufficiently large p, the integrand $M_\ell(w(s), w(t))\,\varphi(\tau(s))\,w'(s)$ vanishes at the end points. Hence a direct application of the quadrature rule (3.14) yields

$$\int_0^1 M_\ell(\tau, \sigma)\psi(\tau)\, d\tau \approx \frac{\pi}{n}\sum_{j=1}^{2n-1} M_\ell(w(s_j), w(t))\,\varphi(\tau(s_j))\,w'(s_j). \tag{3.16}$$

17

3.3.2 Numerical evaluation of (3.12)

From previous discussions, the kernel N_ℓ is not singular when y is away from the slit corners. However, for y near the slit corners, N_ℓ becomes singular. More precisiely, in the xy-coordinate, the singular behavior of the kernel is given by $\Theta(x, y) \sim O(1/|x - y|)$. Hence, a direct application of the trapezoidal rule (3.14) would not lead to a high-oder accuracy for those target points. A modified version of the integral formulation is introduced to remedy the issue. To this end, we introduce the integral operator

$$\mathbb{K}^0[\boldsymbol{\varphi}](y) = \sum_{j=1}^{4} \int_{\Gamma_j} \frac{1}{2\pi} \frac{\partial \ln |x - y|}{\partial \nu_x} \varphi_j(x) \, ds_x \quad y \in \Gamma_i.$$

Let $\mathbf{1}$ be the constant function of 1 along the slit boundary, then

$$\mathbb{K}^0[\mathbf{1}](y) = \frac{1}{2}. \tag{3.17}$$

Let us discuss the evaluation of $\mathbb{K}^e[\boldsymbol{\varphi}]$ for $y \in \Gamma_1$. The treatment for y belonging to other boundaries is the same.

Using the relation (3.17), it follows that

$$\mathbb{K}^e\boldsymbol{\varphi}(y) = \frac{1}{\varepsilon_m + 1} \left(\varphi^{(1)} \cdot \eta^{(1)}(y) + \varphi^{(2)} \cdot \eta^{(2)}(y) \right) \cdot \left(1 - 2\mathbb{K}^0[\mathbf{1}] \right) + \mathbb{K}^e\boldsymbol{\varphi}(y), \quad y \in \Gamma, \tag{3.18}$$

where $\varphi^{(1)}$ and $\varphi^{(2)}$ denotes the value of the density function at the corners $y^{(1)}$ and $y^{(2)}$ as shown in Figure 4. $\eta^{(1)}$ is a smooth cut-off function that attains 1 near the corner $y^{(1)}$ and vanishes toward the other corner $y^{(2)}$. Similarly, the cut-off function $\eta^{(2)}$ is 1 near the corner $y^{(2)}$ and 0 near the corner $y^{(1)}$. We compute $\mathbb{K}^e\boldsymbol{\varphi}(y)$ via the equivalent formulation (3.18). When the target point y is near the corner $y^{(1)}$ such that $\eta^{(1)} = 1$ and $\eta^{(2)} = 0$, the formulation (3.18) reduces to

$$\frac{1}{\varepsilon_m + 1} \varphi^{(1)} \cdot \left(1 - 2\mathbb{K}^0[\mathbf{1}] \right) + \mathbb{K}^e\boldsymbol{\varphi}(y),$$

or more precisely,

$$\frac{1}{\varepsilon_m + 1} \varphi^{(1)} + \sum_{j=1}^{4} \int_{\Gamma_j} \Theta_\ell(x, y) \varphi_j(x) \, ds_x - \varphi^{(1)} \cdot \frac{1}{\pi(\varepsilon_m + 1)} \int_{\Gamma_j} \frac{\partial \ln |x - y|}{\partial \nu_x} \, ds_x.$$

In the above integral, the portion that contains a singular kernel is

$$\frac{1}{\pi(\varepsilon_m + 1)} \int_{\Gamma_3} \frac{\partial \ln |x - y|}{\partial \nu_x} (\varphi(x) - \varphi^{(1)}) \, ds_x, \tag{3.19}$$

and the remaining parts are smooth. However, the whole integrand for (3.19) is not singular, by observing that the smoothness of the function $\varphi(x) - \varphi^{(1)}$ cancels the singularity arising from the kernel $\frac{\partial \ln |x-y|}{\partial \nu_x}$ as x gets closer to the corner $y^{(1)}$. Therefore, we can still apply

graded mesh over the slit boundary and the quadrature rule (3.14) to compute (3.18). This leads to the following discretization formulas

$$\int_0^1 N_\ell(\tau, \sigma) \varphi(\tau) \, d\tau \approx \frac{\pi}{n} \sum_{j=1}^{2n-1} N_\ell(w(s_j), w(t)) \, \varphi(\tau(s_j)) \, w'(s_j), \qquad (3.20)$$

$$\int_0^1 N^{(0)}(\tau, \sigma) \, d\tau \approx \frac{\pi}{n} \sum_{j=1}^{2n-1} N_\ell^{(0)}(w(s_j), w(t)) \, w'(s_j). \qquad (3.21)$$

for each integral in (3.18), where $N^{(0)}(\tau, \sigma)$ denotes the kernel $\frac{\partial \ln |x-y|}{\partial \nu_x}$ in the parameterization space.

4 The strategy for effective initial guess

The initial guess is the key to guarantee the convergence of the Newton's method for solving the eigenvalue problem (2.25) and the robustness of the overall numerical approach. We introduce an approximate model for the original scattering problem (1.1), for which the leading orders of the resonances can be derived and computed at very low cost. Those values are used as initial guesses for computing the resonances.

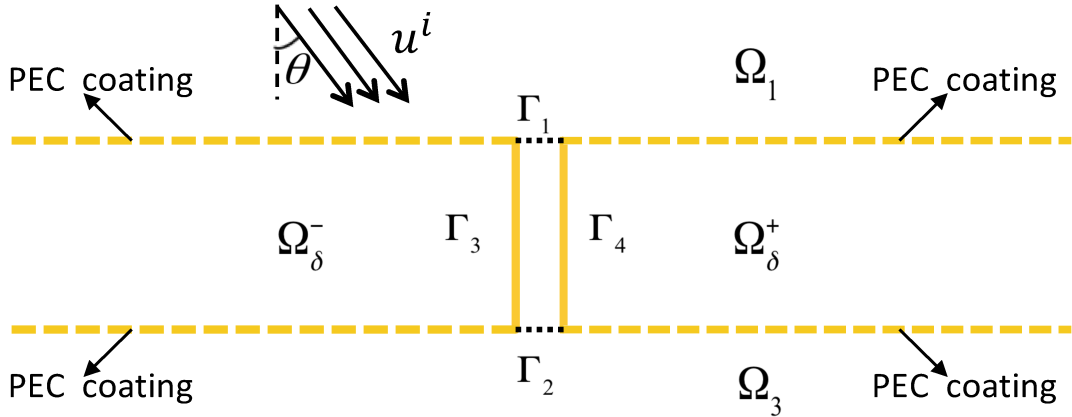## 4.1 An approximate model for the scattering problem

Figure 5: The approximate scattering model where the top and the bottom of the metal (dash lines) are coated with perfectly conducting layers.

We consider an approximate model, where the top and the bottom of the metal (dash lines in Figure 5) are coated with perfectly conducting layers. Recall that $\Omega_\delta = \Omega_\delta^+ \cup \Omega_\delta^-$, correspondingly this leads to zero Neumann boundary condition along metal-vacuum interfaces $\partial\Omega_\delta \backslash (\Gamma_3 \cup \Gamma_4)$. In addition, note that $|\varepsilon_m'| \gg |\varepsilon_m''|$ holds the real and imaginary parts

19

of ε_m, we neglect the metal loss in the approximate model by setting the metal permittivity as ε'_m. As such, the total field $\tilde{u}$ after the scattering satisfies

$$
\begin{cases}
\nabla \cdot \left(\dfrac{1}{\tilde{\varepsilon}(x)} \nabla \tilde{u} \right) + k^2 u = 0 & \text{in } \mathbb{R}^2 \backslash \partial \Omega_\delta, \\[3mm]
[\tilde{u}] = 0, \ \left[\dfrac{1}{\tilde{\varepsilon}} \dfrac{\partial \tilde{u}}{\partial \nu} \right] = 0 & \text{on } \Gamma_3 \cup \Gamma_4, \\[3mm]
\dfrac{\partial \tilde{u}}{\partial \nu} = 0 & \text{on } \partial \Omega_\delta \backslash (\Gamma_3 \cup \Gamma_4),
\end{cases}
\tag{4.1}
$$

where

$$
\tilde{\varepsilon}(x) = \begin{cases}
\varepsilon_0 & x \in \mathbb{R}^2 \backslash \bar{\Omega}_\delta, \\[2mm]
\varepsilon'_m & x \in \Omega_\delta.
\end{cases}
$$

The rationale for proposing the approximate model is as follows. For a given permittivity ε_m, light can penetrate into the metal with a skin depth δ_m. Let us denote the penetration area in the metal by S_{δ_m}, then the slit S_δ together with the penetration area S_{δ_m} serve as a whole resonator, which attains a countable sequence of resonant frequencies. This resonator couples with the exterior medium through the slit aperture and the metal-vacuum interfaces, which would lead to shifts of resonant frequencies. In the case when $\mathrm{Re}\,\varepsilon_m \ll -1$, one may expect that the coupling through the metal-vacuum interfaces is weak and hence the corresponding induced resonance shift is small. A detailed rigorous analysis will be presented in [20]. In the above approximate model, we neglect such coupling and it is expected that corresponding resonances will not be far from the resonances of the original system (1.1). In the rest of this section, we derive the leading-order terms of the resonances for the system (4.1). The argument shares some similarity with the asymptotic analysis of the resonances for a perfectly conducting slit [17]. Thus we skip some technical details but highlight the major differences when the metal is not a perfect conductor anymore.

4.2 Green's functions and boundary integral formulation

4.2.1 Green's functions

Let $g^e(x, y)$ be the exterior Green's function for the PEC slab that satisfies

$$
\begin{cases}
\Delta g^e(x, y) + k^2 g^e(x, y) = \tilde{\delta}(x - y) & x, y \in \Omega_\ell, \ell = 1, 2 \\[3mm]
\dfrac{\partial g^e(x, y)}{\partial \nu_x} = 0 & \text{on } \partial \Omega_\ell.
\end{cases}
$$

Then

$$
g^e(x, y) = -\frac{i}{4} \left(H_0^{(1)}(k|x - y|) + H_0^{(1)}(k|x - y'|) \right),
$$

where $H_0^{(1)}$ is the first kind Hankel function of order 0, and

$$
y' = \begin{cases}
(y_1, 2 - y_2) & \text{if } x, y \in \Omega_1, \\[2mm]
(y_1, -y_2) & \text{if } x, y \in \Omega_2.
\end{cases}
$$

We also introduce the interior Green's functions $g^i(x, y)$ for the metal-vacuum-metal waveguide that satisfies

$$
\begin{cases}
\nabla \cdot \left(\dfrac{1}{\tilde{\varepsilon}(x)} \nabla g^i(x, y) \right) + k^2 g^i(x, y) = 0 = \tilde{\delta}(x - y) & x \in \Omega_2, y \in S_\delta, \\[2mm]
\dfrac{\partial g^i(x, y)}{\partial \nu_x} = 0 & \text{on } \{x_2 = 1\} \cup \{x_2 = 0\}.
\end{cases}
$$

Using eigenfunctions along the x_2 direction, $g^i(x, y)$ can be expressed as

$$
g^i(x, y) = \sum_{n=0}^{\infty} \tilde{\omega}_n \, g_n(x_1, y_1) \, \cos(n\pi x_2) \cos(n\pi y_2), \tag{4.2}
$$

where the coefficients

$$
\tilde{\omega}_n = \begin{cases} 1 & n = 0, \\ 2 & n \geq 1, \end{cases}
$$

and the 1D Green's function $g_n(x_1, y_1)$ solves

$$
\mathcal{L}_n g_n(x_1, y_1) := \left(\frac{1}{\tilde{\varepsilon}(x_1)} g_n'(x_1, y_1) \right)' + \left(k^2 - \frac{(n\pi)^2}{\tilde{\varepsilon}(x_1)} \right) g_n(x_1, y_1) = \tilde{\delta}(x_1 - y_1),
$$
$$
-\infty < x_1 < \infty, \quad 0 < y_1 < \delta.
$$

It is known that the delta function adopts the following eigenfunction expansion (cf. [17]):

$$
\tilde{\delta}(x_1 - y_1) = \frac{1}{\delta} + \sum_{m=1}^{\infty} \frac{2}{\delta} \cos\left(\frac{m\pi x_1}{\delta} \right) \cos\left(\frac{m\pi y_1}{\delta} \right) \quad \text{for } x_1, y_1 \in (0, \delta).
$$

Let $\chi_{(0,\delta)}(x_1)$ be the characteristic function on $(0, \delta)$, then we can split $g_n(x_1, y_1)$ as

$$
g_n(x_1, y_1) = g_n^{(0)}(x_1) + g_n^{(1)}(x_1, y_1). \tag{4.3}
$$

where

$$
\mathcal{L}_n g_n^{(0)}(x_1, y_1) = \frac{1}{\delta} \cdot \chi_{(0,\delta)}(x_1), \tag{4.4}
$$

$$
\mathcal{L}_n g_n^{(1)}(x_1, y_1) = \frac{2}{\delta} \cdot \sum_{m=1}^{\infty} \cos\left(\frac{m\pi x_1}{\delta} \right) \cos\left(\frac{m\pi y_1}{\delta} \right) \cdot \chi_{(0,\delta)}(x_1). \tag{4.5}
$$

It follows by a direct calculation that

$$
g_n^{(0)}(x_1) = \begin{cases}
\dfrac{1}{\delta} \cdot c_{n1} e^{\gamma_n x_1}, & -\infty < x_1 < 0, \\[3mm]
\dfrac{1}{\delta} \cdot c_{n1} e^{\gamma_n (x_1 - \delta)}, & x_1 > \delta, \\[3mm]
\dfrac{1}{\delta} \cdot \left[c_{n2} \left(e^{i\alpha_n x_1} + e^{i\alpha_n (\delta - x_1)} \right) + \dfrac{1}{k^2 - (n\pi)^2} \right], & 0 < x_1 < \delta,
\end{cases}
$$

21

where $\gamma_n = \sqrt{(n\pi)^2 - k^2 \varepsilon'_m}$, $\alpha_n = \sqrt{k^2 - (n\pi)^2}$, and the coefficients

$$c_{n2} = \frac{\gamma_n}{\alpha_n^2} \cdot \frac{1}{i\alpha_n \varepsilon'_m(1 - e^{i\alpha_n \delta}) - \gamma_n(1 + e^{i\alpha_n \delta})}, \quad c_{n1} = (1 + e^{i\alpha_n \delta})c_{n2} + \frac{1}{k^2 - (n\pi)^2}.$$

Lemma 4.1 *If $\delta \ll 1$ and $|\varepsilon'_m| \sim O(1/\delta)$, then the following holds for $x_1 \in (0, \delta)$:*

$$\sum_{n=0}^{\infty} \tilde{\omega}_n \, g_n^{(0)}(x_1) = \beta_{i,1} + O(1), \quad \sum_{n=0}^{\infty} (-1)^n \tilde{\omega}_n \, g_n^{(0)}(x_1) = \beta_{i,2} + O(1).$$

Here $\beta_{i,1}$ and $\beta_{i,2}$ are constants given by

$$\beta_{i,1}(k) = \frac{1}{\delta} \cdot \sum_{n=1}^{\infty} \tilde{\omega}_n \left(\left(1 + e^{i\alpha_n \delta}\right) c_{n,2} + \frac{1}{k^2 - (n\pi)^2} \right), \tag{4.6}$$

$$\beta_{i,2}(k) = \frac{1}{\delta} \cdot \sum_{n=1}^{\infty} (-1)^n \tilde{\omega}_n \left(\left(1 + e^{i\alpha_n \delta}\right) c_{n,2} + \frac{1}{k^2 - (n\pi)^2} \right). \tag{4.7}$$

Proof We split the sum $\displaystyle\sum_{n=0}^{\infty} \tilde{\omega}_n \, g_n^{(0)}(x_1)$ as

$$\sum_{n=0}^{\infty} \tilde{\omega}_n \, g_n^{(0)}(x_1) = \sum_{n=0}^{N_0} \tilde{\omega}_n \, g_n^{(0)}(x_1) + \sum_{n=N_0}^{\infty} \tilde{\omega}_n \, g_n^{(0)}(x_1),$$

where $N_0 = O(\delta^{-1/2})$. If $n \sim O(\delta^{-\mu_n})$ and $0 \le \mu_n \le 1/2$, the Taylor expansion gives

$$e^{i\alpha_n x_1} + e^{i\alpha_n(\delta - x_1)} = 1 + e^{i\alpha_n \delta} + O(\delta^{1-\mu_n}) \quad \text{for } x_1 \in (0, \delta).$$

On the other hand, it is clear that

$$c_{n,2} \sim O(1/\alpha_n^2) \sim O(\delta^{2\mu_n}) \quad \text{for } 0 \le n \le N_0.$$

Therefore,

$$\sum_{n=0}^{N_0} \tilde{\omega}_n \, g_n^{(0)}(x_1) = \frac{1}{\delta} \cdot \sum_{n=0}^{N_0} \tilde{\omega}_n \left(\left(1 + e^{i\alpha_n \delta}\right) c_{n,2} + \frac{1}{k^2 - (n\pi)^2} + O(\delta^{1+\mu_n}) \right). \tag{4.8}$$

For $n > N_0$, in light of $|\varepsilon'_m| \sim O(1/\delta)$, it follows that

$$c_{n,2} \sim O\left(1/(\alpha_n^2 |\varepsilon'_m|)\right) \sim O\left(1/(n^2 \delta)\right).$$

We obtain

$$\sum_{n=N_0}^{\infty} \tilde{\omega}_n \, g_n^{(0)}(x_1) = \frac{1}{\delta} \cdot \sum_{n=N_0}^{\infty} \tilde{\omega}_n \left(\left(1 + e^{i\alpha_n \delta}\right) c_{n,2} + \frac{1}{k^2 - (n\pi)^2} \right) + O(1). \tag{4.9}$$

The assertion holds by combining (4.8) and (4.9). $\qquad\square$

22

We expand $g_n^{(1)}(x_1, y_1)$ as the sum of eigenfunctions $\{v_{np}\}_{p=1}^{\infty}$ for the operator $\mathcal{L}_n$ (see Appendix C). For a given small δ, let us assume that $|\varepsilon_m'| \sim O(1/\delta)$. Then it follows from Lemma C.1 that

$$v_{np}(x_1) = \sqrt{\frac{2}{\delta}} \left(\cos\left(\frac{(p+1)\pi x_1}{\delta}\right) + O(\delta^s) \right) \quad \text{for } x_1 \in (0, \delta),$$

where $s \geq 1/2$. On the other hand, from Lemma C.1, each eigenfunction $v_{np}(x_1)$ decays with a rate of $O\left(e^{-\sqrt{|\varepsilon_m'|}/\delta}\right)$ outside the interval $(0, \delta)$. Therefore, recall that $g_n^{(1)}(x_1, y_1)$ satisfies (4.5), we may approximate $g_n^{(1)}(x_1, y_1)$ by $\tilde{g}_n^{(1)}(x_1, y_1)$, where $\tilde{g}_n^{(1)}(x_1, y_1)$ satisfies

$$\mathcal{L}_n \tilde{g}_n^{(1)}(x_1, y_1) = \sum_{p=0}^{\infty} v_{np}(x_1) v_{np}(y_1).$$

Using the fact that $\mathcal{L}_n v_{np} = (k^2 - \lambda_{np}) v_{np}$, where λ_{np} is the eigenvalue for $\mathcal{L}_n$, it follows that

$$\tilde{g}_n^{(1)}(y_1, y_1) = \sum_{p=0}^{\infty} \frac{1}{k^2 - \lambda_{np}} v_{np}(x_1) v_{np}(y_1), \quad x_1, y_1 \in (0, \delta). \tag{4.10}$$

We skip the very technical proof and summarize the above formal analysis in the following lemma.

Lemma 4.2 *If $\delta \ll 1$ and $|\varepsilon_m'| \sim O(1/\delta)$, then for each n, it holds that*

$$g_n^{(1)}(y_1, y_1) = \tilde{g}_n^{(1)}(y_1, y_1) + O(\delta^\varsigma) \quad \text{for } x_1, y_1 \in (0, \delta),$$

where $\varsigma \geq 1$ and $\tilde{g}_n^{(1)}$ is defined in (4.10).

4.2.2 Boundary integral formulation

Let $\tilde{u}^r$ be the reflected field by the perfectly conducting slab in the absence of slit, and $\tilde{u}^s := \tilde{u} - u^i - \tilde{u}^r$ be the scattered field induced by opening the slit. From the Green's identity, one obtains an integral equation for $\tilde{u}^s$:

$$\tilde{u}^s(y) = \int_{\Gamma_1} g^e(x, y) \frac{\partial \tilde{u}^s(x)}{\partial \nu} ds_x, \quad y \in \Omega_1.$$

Using the fact that $\dfrac{\partial u^i}{\partial \nu} + \dfrac{\partial u^r}{\partial \nu} = 0$ on $\{x_2 = 1\}$ and the continuity of the single layer potential, it follows that the total field satisfies

$$\tilde{u}(y) = \int_{\Gamma_1} g^e(x, y) \frac{\partial \tilde{u}(x)}{\partial \nu} ds_x + u^i(y) + \tilde{u}^r(y), \quad y \in \Gamma_1.$$

Similarly,

$$\tilde{u}(y) = \int_{\Gamma_2} g^e(x, y) \frac{\partial \tilde{u}(x)}{\partial \nu} ds_x, \quad y \in \Gamma_2.$$

Applying the Green's identity in the slab domain Ω_2 and using the boundary conditions, the solution inside the slit can be expressed as

$$\tilde{u}(y) = -\int_{\Gamma_1 \cup \Gamma_2} g^i(x,y)\frac{\partial \tilde{u}(x)}{\partial \nu}ds_x \quad \text{for } y \in S_\delta.$$

This leads to the equation

$$\tilde{u}(y) = -\int_{\Gamma_1 \cup \Gamma_2} g^i(x,y)\frac{\partial \tilde{u}(x)}{\partial \nu}ds_x \quad \text{for } x \in \Gamma_1 \cup \Gamma_2.$$

Imposing the continuity of the solution along the slit apertures leads to the following system of integral equations:

$$\begin{cases} \displaystyle\int_{\Gamma_1} g^e(x,y)\frac{\partial \tilde{u}}{\partial \nu}ds_x + \int_{\Gamma_1 \cup \Gamma_2} g^i(x,y)\frac{\partial \tilde{u}}{\partial \nu}ds_x + u^i + \tilde{u}^r = 0 \quad \text{on } \Gamma_1, \\[4mm] \displaystyle\int_{\Gamma_2} g^e(x,y)\frac{\partial \tilde{u}}{\partial \nu}ds_x + \int_{\Gamma_1 \cup \Gamma_2} g^i(x,y)\frac{\partial \tilde{u}}{\partial \nu}ds_x = 0 \quad \text{on } \Gamma_2. \end{cases} \tag{4.11}$$

To study the resonances of the scattering problem, it is more convenient to rescale the formulation by introducing the variables $X = x_1/\delta$ and $Y = y_1/\delta$. We also define the following quantities:

$$\tilde{\varphi}_1(X) := -\frac{\partial \tilde{u}}{\partial x_2}(\delta X, 1); \quad \tilde{\varphi}_2(Y) := \frac{\partial \tilde{u}}{\partial x_2}(\delta X, 0);$$
$$\tilde{f}(X) := (u^i + u^r)(\delta X, 1) = 2e^{ikd_1\delta X};$$
$$G^e(X,Y) := g^e(\delta X, 1; \delta Y, 1) = g^e(\delta X, 0; \delta Y, 0);$$
$$G^i(X,Y) := g^i(\delta X, 1; \delta Y, 1) = g^i(\delta X, 0; \delta Y, 0)$$
$$\tilde{G}^i(X,Y) := g^i(\delta X, 1; \delta Y, 0) = g^i(\delta X, 0; \delta Y, 1).$$

Then the boundary integral equations (4.11) can be written as the following in the scaled coordinates.

$$\begin{bmatrix} T^e + T^i & \tilde{T}^i \\ \tilde{T}^i & T^e + T^i \end{bmatrix}\begin{bmatrix} \tilde{\varphi}_1 \\ \tilde{\varphi}_2 \end{bmatrix} = \begin{bmatrix} \tilde{f}/\delta \\ 0 \end{bmatrix}, \tag{4.12}$$

where

$$(T^e\varphi)(Y) = \int_0^1 G^e_\delta(X,Y)\varphi(X)dX \quad Y \in (0,1); \tag{4.13}$$

$$(T^i\varphi)(Y) = \int_0^1 G^i_\delta(X,Y)\varphi(X)dX \quad Y \in (0,1); \tag{4.14}$$

$$(\tilde{T}^i\varphi)(Y) = \int_0^1 \tilde{G}^i_\delta(X,Y)\varphi(X)dY \quad Y \in (0,1). \tag{4.15}$$

4.3 Asymptotic expansions of the boundary integral operators

We have the following asymptotic expansions for the kernels G^i, G^e and $\tilde{G}^i$.

Lemma 4.3 *If $k\delta \ll 1$, then for $X, Y \in (0,1)$,*

$$G^e(X,Y) + G^i(X,Y) = \beta(k) + \kappa(X,Y) + k_\infty(X,Y), \tag{4.16}$$
$$\tilde{G}^i(X,Y) = \tilde{\beta}(k) + \tilde{k}_\infty(X,Y). \tag{4.17}$$

In the above,

$$\beta(k) = \left(\frac{1}{\pi}(\ln k + \tilde{\gamma}_0) + \frac{1}{\pi}\ln\delta \right) + \beta_{i,1}(k), \quad \tilde{\beta} = \beta_{i,2}(k), \tag{4.18}$$

where $\beta_{i,1}$ and $\beta_{i,2}$ are defined in (4.6) and (4.7), $\tilde{\gamma}_0 = c_0 - \ln 2 - i\pi/2$, and c_0 is the Euler constant. The kernel $|\kappa(X,Y)| \sim O(1)$, $|k_\infty(X,Y)| \sim O(\delta^\varsigma)$ and $|\tilde{k}_\infty(X,Y)| \sim O(\delta^\varsigma)$ where $\varsigma \geq 1$.

Proof First, the asymptotic expansion of $H_0^{(1)}$ (cf. [10]) leads to

$$G^e(X,Y) = \left(-\frac{i}{2} \right) H_0^{(1)}(\delta k |X - Y|)$$

$$= \frac{1}{\pi} \left[\ln\delta + \ln k + \tilde{\gamma}_0 + \ln|X - Y| + O\left(\delta^2 \ln\delta\right) \right]. \tag{4.19}$$

From the expansion (4.2) and the decomposition (4.3), we have

$$G^i(X,Y) = \sum_{n=0}^{\infty} \tilde{\omega}_n \, g_n(\delta X, \delta Y) = \sum_{n=0}^{\infty} \tilde{\omega}_n \, g_n^{(0)}(\delta X) + \sum_{n=0}^{\infty} \tilde{\omega}_n \, g_n^{(1)}(\delta X, \delta Y).$$

An application of Lemma 4.1 and 4.2 yields

$$G^i(X,Y) = \beta_{i,1}(k) + O(1) + \sum_{n=0}^{\infty} \tilde{\omega}_n \, \tilde{g}_n^{(1)}(\delta X, \delta Y) + O(\delta^\varsigma) \tag{4.20}$$

for $\varsigma \geq 1$. By the definition (4.10), it follows that

$$\sum_{n=0}^{\infty} \tilde{\omega}_n \, \tilde{g}_n^{(1)}(\delta X, \delta Y) = \sum_{n=0}^{\infty}\sum_{p=0}^{\infty} \frac{\tilde{\omega}_n}{k^2 - \lambda_{np}} v_{np}(\delta X) v_{np}(\delta Y)$$

$$= \sum_{p=1}^{\infty}\sum_{n=0}^{\infty} \frac{2\tilde{\omega}_n}{(k^2 - \lambda_{np}) \cdot \delta} \Big(\cos(p\pi X)\cos(p\pi Y) + O(\delta^\varsigma) \Big), \tag{4.21}$$

where we have used the following fact in the second equality

$$v_{np}(\delta X) = \sqrt{\frac{2}{\delta}} \left(\cos\left((p+1)\pi X \right) + O(\delta^s) \right) \quad \text{for } s \geq 1/2.$$

For each p, from the asymptotic expansion of the λ_{np} (C.2) and the representation of elementary functions by series (cf. [13]), the constant

$$\sum_{n=0}^{\infty} \frac{2\tilde{\omega}_n}{(k^2 - \lambda_{np}) \cdot \delta} \approx -\frac{2}{\delta \cdot \sqrt{((p\pi + \theta_0)/\delta)^2 - k^2}} \coth\left(\sqrt{((p\pi + \theta_0)/\delta)^2 - k^2}\right)$$

$$\approx -\frac{1}{p\pi} - \frac{k^2\delta^2}{p^3\pi^3} + O\left(\frac{\delta^4}{p^5}\right).$$

By substituting into (4.21), we see that

$$\sum_{n=0}^{\infty} \tilde{\omega}_n \, \tilde{g}_n^{(1)}(\delta X, \delta Y) = \sum_{p=1}^{\infty} \frac{2}{p\pi} \cos(p\pi X) \cos(p\pi Y) + O(\delta^\varsigma). \tag{4.22}$$

A combination of (4.19), (4.20), (4.22) leads to the expansion for $G^e(X, Y) + G^i(X, Y)$.

For $\tilde{G}^i(X, Y)$, from Lemma 4.1 and 4.2, we see that

$$\tilde{G}^i(X, Y) = \beta_{i,2}(k) + O(1) + \sum_{n=0}^{\infty} (-1)^n \tilde{\omega}_n \, \tilde{g}_n^{(1)}(\delta X, \delta Y) + O(\delta^\varsigma). \tag{4.23}$$

A similar calculation as above gives the desired expansion, and we omit here for conciseness.
□

Based on the above decomposition of the Green's functions, we have the decomposition of the following integral operators:

Lemma 4.4 *Let K, K_∞, $\tilde{K}_\infty$ be the integral operators corresponding to the Schwarz kernels $\kappa(X, Y)$, $\kappa_\infty(X, Y)$ and $\tilde{\kappa}_\infty(X, Y)$, and P be projection operator defined by $P\varphi(X) = (\varphi, 1)1$, then the operator $T^e + T^i$ and $\tilde{T}^i$ admit the following decomposition:*

$$T^e + T^i = \beta P + K + K_\infty, \quad \tilde{T}^i = \tilde{\beta}P + \tilde{K}_\infty.$$

4.4 Scattering resonances of the approximate model and the strategy for initial guess

To obtain the resonances of the approximate model (4.1), we solve for the homogeneous problem when $\tilde{f} = 0$ in (4.12). By virtue of Lemma 4.4, the integral operators adopts the following expansion:

$$\begin{bmatrix} T^e + T^i & \tilde{T}^i \\ \tilde{T}^i & T^e + T^i \end{bmatrix} = \begin{bmatrix} \beta P & \tilde{\beta} P \\ \tilde{\beta} P & \beta P \end{bmatrix} + K\mathbb{I} + \begin{bmatrix} K_\infty & \tilde{K}_\infty \\ \tilde{K}_\infty & K_\infty \end{bmatrix} =: \mathbb{P} + \mathbb{L},$$

where

$$\mathbb{P} = \begin{bmatrix} \beta P & \tilde{\beta} P \\ \tilde{\beta} P & \beta P \end{bmatrix}, \quad \mathbb{K}_\infty = \begin{bmatrix} K_\infty & \tilde{K}_\infty \\ \tilde{K}_\infty & K_\infty \end{bmatrix} \quad \text{and} \quad \mathbb{L} = K\mathbb{I} + \mathbb{K}_\infty.$$

The homogeneous problem $(\mathbb{P} + \mathbb{L})\varphi = 0$ can be rewritten as

$$\mathbb{L}^{-1}\,\mathbb{P}\,\tilde{\varphi} + \tilde{\varphi} = 0. \tag{4.24}$$

Let $\mathbf{e}_1 = [1, 0]^T$ and $\mathbf{e}_2 = [0, 1]^T$. By expressing $\mathbb{P}\,\tilde{\varphi}$ explicitly and taking the inner product of (4.24) with $\mathbf{e}_1$ and $\mathbf{e}_2$ respectively, the homogeneous problem reduces to (cf. [17])

$$(\mathbb{M} + \mathbb{I}) \begin{bmatrix} \langle \varphi, \mathbf{e}_1 \rangle \\ \langle \varphi, \mathbf{e}_2 \rangle \end{bmatrix} = 0,$$

where

$$\mathbb{M} = \beta \begin{bmatrix} \langle \mathbb{L}^{-1}\mathbf{e}_1, \mathbf{e}_1 \rangle & \langle \mathbb{L}^{-1}\mathbf{e}_1, \mathbf{e}_2 \rangle \\ \langle \mathbb{L}^{-1}\mathbf{e}_1, \mathbf{e}_2 \rangle & \langle \mathbb{L}^{-1}\mathbf{e}_1, \mathbf{e}_1 \rangle \end{bmatrix} + \tilde{\beta} \begin{bmatrix} 0 & 1 \\ 1 & 0 \end{bmatrix} \begin{bmatrix} \langle \mathbb{L}^{-1}\mathbf{e}_1, \mathbf{e}_1 \rangle & \langle \mathbb{L}^{-1}\mathbf{e}_1, \mathbf{e}_2 \rangle \\ \langle \mathbb{L}^{-1}\mathbf{e}_1, \mathbf{e}_2 \rangle & \langle \mathbb{L}^{-1}\mathbf{e}_1, \mathbf{e}_1 \rangle \end{bmatrix}$$

The eigenvalues for $\mathbb{M} + \mathbb{I}$ are

$$\lambda_1(k) = 1 + (\beta(k) + \tilde{\beta}(k)) \left(\langle \mathbb{L}^{-1}\mathbf{e}_1, \mathbf{e}_1 \rangle + \langle \mathbb{L}^{-1}\mathbf{e}_1, \mathbf{e}_2 \rangle \right), \tag{4.25}$$
$$\lambda_2(k) = 1 + (\beta(k) - \tilde{\beta}(k)) \left(\langle \mathbb{L}^{-1}\mathbf{e}_1, \mathbf{e}_1 \rangle - \langle \mathbb{L}^{-1}\mathbf{e}_1, \mathbf{e}_2 \rangle \right). \tag{4.26}$$

The associated eigenvectors are

$$\begin{bmatrix} 1 & 1 \end{bmatrix}^T \quad \text{and} \quad \begin{bmatrix} 1 & -1 \end{bmatrix}^T. \tag{4.27}$$

Therefore, the scattering resonances of the problem (4.1), or equivalently, the characteristic values of the operator-valued function $\mathbb{P} + \mathbb{L}$, are the roots of the two analytic functions $\lambda_1(k)$ and $\lambda_2(k)$. The leading order of the resonances are stated in the following theorem.

Theorem 4.5 *If $\delta \ll 1$, there exist two sets of resonances, $\{k_{\ell,1}\}_{\ell=1}^{\infty}$ and $\{k_{\ell,2}\}_{\ell=1}^{\infty}$, for the scattering problem (4.1), and the following asymptotic expansions hold:*

$$k_{\ell,1} = k_{\ell,1}^{(0)} - \frac{1}{\pi q_1'\left(k_{\ell,1}^{(0)}\right)} \cdot \delta \ln \delta + O(\delta^{\varsigma}), \quad k_{\ell,2} = k_{\ell,2}^{(0)} + \frac{1}{\pi q_2'\left(k_{\ell,2}^{(0)}\right)} \cdot \delta \ln \delta + O(\delta^{\varsigma}), \quad \varsigma \geq 1$$

for $\ell\delta \ll 1$. The leading-oder terms $k_{\ell,1}^{(0)}$ and $k_{\ell,2}^{(0)}$ are the roots of real-valued functions $q_1(k)$ and $q_2(k)$ respectively, where

$$q_1(k) = \delta\left(\beta_{i,1}(k) + \beta_{i,2}(k)\right), \quad q_2(k) = \delta\left(\beta_{i,1}(k) - \beta_{i,2}(k)\right).$$

Proof. From the expression of the eigenvalue in (4.25), and the definition of $\beta(k)$ and $\tilde{\beta}(k)$ in (4.18), the roots of $\lambda_1(k)$ satisfy

$$1 + \left[\frac{q_1(k)}{\delta} + \frac{1}{\pi}\ln\delta + \frac{1}{\pi}(\ln k + \tilde{\gamma}_0) \right] \left(\langle \mathbb{L}^{-1}\mathbf{e}_1, \mathbf{e}_1 \rangle + \langle \mathbb{L}^{-1}\mathbf{e}_1, \mathbf{e}_2 \rangle \right) = 0.$$

We investigate the roots for the leading order terms of $\lambda_1(k)$, which is given by $\dfrac{q_1(k)}{\delta} + \dfrac{1}{\pi}\ln\delta$. This leads to solving the following equation:

$$q_1(k) + \frac{1}{\pi}\delta \ln \delta = 0,$$

and its roots are given by

$$\hat{k}_{\ell,1} = k_{\ell,1}^{(0)} - \frac{1}{\pi q_1' \left(k_{\ell,1}^{(0)} \right)} \cdot \delta \ln \delta + O(\delta^2 \ln^2 \delta).$$

An application of Rouche's theorem gives the desired expansion for $\lambda_1(k) = 0$. The roots of $\lambda_2(k)$ can be obtained by a parallel argument. $\qquad\square$

Denote the initial guesses for computing the resonances of (2.25) as

$$\tilde{k}_\ell = \tilde{k}_\ell' + i\,\tilde{k}_\ell'', \quad \ell = 1, 2, 3, \cdots, L.$$

When $k_{\ell,j}^{(0)}\delta < 1$, we use the first two terms in the above expansions, $k_{\ell,j}^{(0)} - \frac{1}{\pi q_j'\left(k_{\ell,j}^{(0)}\right)} \cdot \delta \ln \delta$ ($j = 1, 2$), as the real parts of the initial guesses. Otherwise, the real parts of the initial guesses are set as the leading-order values $k_{\ell,j}^{(0)}$ ($j = 1, 2$). Let the real parts, $\{\tilde{k}_\ell\}_{\ell=1}^L$, be those values ordered increasingly. Although explicit asymptotic expansion for the imaginary part of resonances are not derived explicitly in Lemma 4.5, it is known that true resonances are located in the fourth quadrant of the complex plane. Using the fact the resonances for the PEC slit has an oder of $O(\delta)$ if $\delta \ll 1$ (cf. (6.1)), it is expected that similar asymptotic expansions will hold for real metals. Hence we choose the imaginary part of the first initial guess as $\tilde{k}_1'' = -\delta$. For $\ell \geq 1$, by observing that the field enhancement is weaker as the frequency becomes higher, we set $\tilde{k}_{\ell+1}'' = -\max_{1 \leq p \leq \ell} |\tilde{k}_p''|$. For the eigenmode (resonant modes) ψ in (2.25), note that the eigenvectors for $\mathbb{M}+\mathbb{I}$ are given by (4.27). Correspondingly, we choose the initial guesses for the resonant modes $\tilde{\psi}_{\ell,j}$ are set as $[1, 1, 0, 0]$ and $[1, -1, 0, 0]$ for $j = 1, 2$, respectively.

5 Numerical examples

In this section, we present various numerical examples to demonstrate the accuracy and effectiveness of the computational approach. We first validate the accuracy of the integral equation method by comparing the computational results with the ones obtained via the vertical mode matching scheme [14, 21, 22]. The integral equation approach with the initial guess strategy is then applied to solve for the resonances of the scattering problem with various slit sizes and permittivity values. In the rest of this section, n_1 and n_2 denotes the number of grid points used to discretize the single and double layer integrals (3.15), (3.16), (3.20) and (3.21) over the horizontal and vertical slit boundaries, respectively.

Example 1 We validate the accuracy of the integral equation method in this example. Let the permittivity for the metal be $\varepsilon_m = -100 + 10i$, and consider the metallic structure with the slit size $\delta = 0.1$ and $\delta = 0.05$, respectively. We solve the scattering problem with an normal incident plane wave u^i. To this end, the single and double layer integrals (3.10) - (3.12) are computed by the quadrature rules (3.15) (3.16), (3.20), and (3.21), using $n_1 = 20$ and $n_2 = 120$ for the horizontal and vertical slit boundaries, respectively. Figures 6 and 7 (left) show the trasmittance T over the frequency band $\{k \mid k \in [1, 10]\}$ for the slit size $\delta = 0.1$

and $\delta = 0.05$, which are obtained by solving the integral equation (2.24). The tranmsittance is defined as $T = P/P_{inc}$, where P is the total power over the bottom gap aperture Γ_2 and P_{inc} is the incident power over the aperture Γ_2. For comparison we apply the vertical mode matching scheme [14, 21, 22] to the solve the scattering problem (1.1) with sufficient number of modes. Figures 6 and 7 (right) plot the difference between the transmittances obtained by two numerical approaches, where the quantity e_T is defined by $e_T = |T - T_{vm}|/|T_{vm}|$ and T_{vm} is the transmittance computed from the vertical mode matching method. It observed that three digits of accuracy is achieved by the integral equation method with the specified grid points.
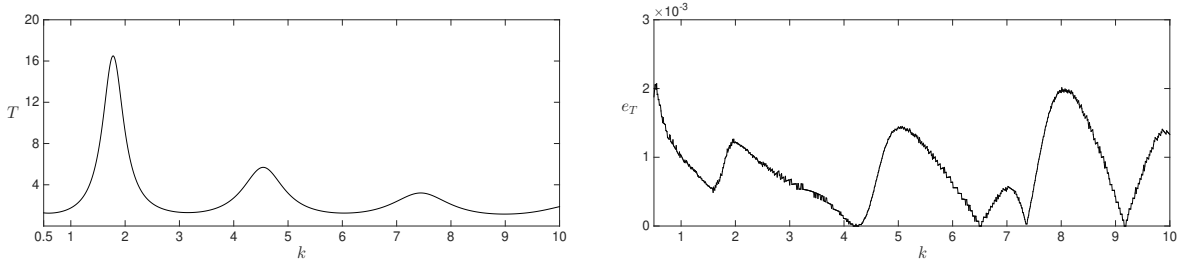

Figure 6: The transmittance T over the frequency band $\{k \,|\, k \in [1, 10]\}$ computed via the integral equation approach (left) and the difference between the transmittance T obtained by two methods (right). $\delta = 0.1$.

Figure 7: The transmittance T over the frequency band $\{k \,|\, k \in [1, 10]\}$ computed via the integral equation approach (left) and the difference between the transmittance T obtained by two methods (right). $\delta = 0.05$.
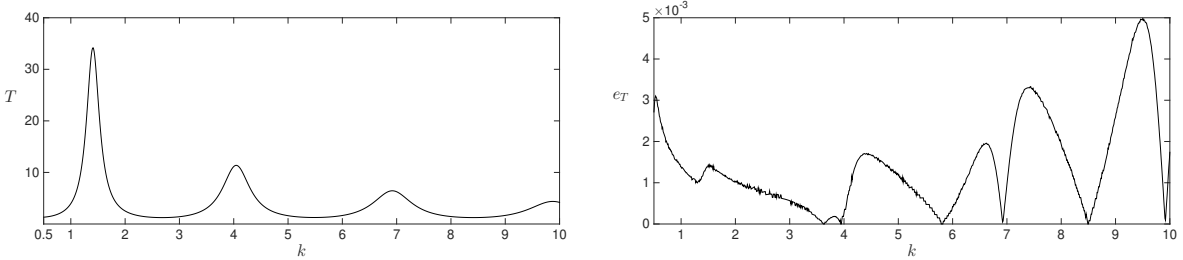
Example 2 The permittivity for the metal is set as $\varepsilon_m = -100 + 10i$. We compute the resonances for the slit size $\delta = 0.02$, 0.05, 0.1, and 0.2, respectively. To discretize the integrals (3.10) and (3.12), $n_1 = 20$ and $n_2 = 80$ are used for the horizontal and vertical slit boundaries respectively. The tolerance is set as 10^{-4} for the Newton solver of the eigenvalue problem (2.25).

The first column of Tables 2 - 5 are the initial-guess values $\{\tilde{k}_\ell\}_{\ell=1}^L$ obtained from the strategy discussed in Section 4 for given δ values. The second and the third column of Tables 2 - 5 show the computed resonances $\{k_\ell\}_{\ell=1}^L$ and the corresponding iteration numbers needed to achieve the desired tolerance. In the tables, the resonances are ordered with increasing real part. We see that the initial guesses indeed provide good approximations of true resonances, especially for lower frequencies and smaller slit sizes where the leading

29

orders of the asymptotic expansions in Theorem 4.5 are more accurate. In addition, from the provided initial-guess values, the Newton solver converges with the given tolerance in only a few iterations (mostly less than 10 iterations). Hence the proposed computational approach is very efficient for obtaining the resonances of the scattering problem.

In order to demonstrate the accuracy of the computed resonances, in Figure 8 we plot the trasmittance T over the frequency band $\{k \mid k \in [0.5, 15]\}$ when a normal incident plane wave u^i impinges on the metallic structure with various slit sizes. When the incident frequency is close to the real part of certain scattering resonance k_ℓ such that the corresponding resonant mode is excited, it is expected that the transmission peaks will occur as long as the magnitude for the imaginary part of k_ℓ is sufficiently small. It is seen from Table 2 - 5 that the real parts of resonances correctly reflect the peaks of transmssions in Figure 8, which validates the accuracy of computed resonances. On the other hand, the smaller the magnitude for the imaginary part of resonances, the higher the transimttance peaks are. This is also consistent with the resonant scattering mechanism.

We would also like to remark on the robustness of the numerical approach by the observation that (i) the iterative eigen-solver indeed converges with the obtained initial-guess values; (ii) for each δ, all resonances in the above frequency band that lie in the vicinity of the real axis have been successfully solved, since each peak in Figure 8 corresponds to one resonance in Table 2 - 5.

Finally, we study the convergence behavior of the numerical method with increasing grid points over the slit boundary. To this end, let us set $\delta = 0.02$ and 0.1 respectively. Table 6 and 7 give the computed resonances with various n_1 and n_2 values. We observe the convergence of the computed values when the mesh is refined. Furthermore, two digits of accuracy is obtained when $n_1 = 20$ and $n_2 = 80$, and three digits of accuracy is obtained when $n_1 = 40$ and $n_2 = 160$.

Table 2: Initial guesses and the computed resonances for $\delta = 0.02$.

$\tilde{k}_\ell$	k_ℓ	iteration numbers
$0.7875 - 0.02i$	$0.7832 - 0.0479i$	7
$2.7481 - 0.0479i$	$2.7513 - 0.1642i$	8
$5.2174 - 0.1642i$	$5.2983 - 0.1847i$	7
$7.9051 - 0.1847i$	$8.0485 - 0.3196i$	8
$10.6994 - 0.3196i$	$10.8462 - 0.3399i$	8
$13.5527 - 0.3399i$	$13.8351 - 0.4129i$	8

Table 3: Initial guesses and the computed resonances for $\delta = 0.05$.

$\tilde{k}_\ell$	k_ℓ	iteration numbers
$1.4590 - 0.05i$	$1.4524 - 0.0765i$	5
$4.0096 - 0.0765i$	$4.0653 - 0.2548i$	5
$6.7421 - 0.2548i$	$6.9522 - 0.3069i$	6
$9.5288 - 0.3069i$	$9.9177 - 0.4572i$	8
$12.3391 - 0.4572i$	$12.8852 - 0.5190i$	9

Table 4: Initial guesses and the computed resonances for $\delta = 0.1$.

$\tilde{k}_\ell$	k_ℓ	iteration numbers
$1.8528 - 0.1i$	$1.8501 - 0.1311i$	5
$4.4502 - 0.1311i$	$4.585 - 0.3882i$	5
$7.1092 - 0.3882i$	$7.5187 - 0.5136i$	6
$11.6860 - 0.5136i$	$10.4920 - 0.7154i$	7
$14.7178 - 0.7154i$	$13.5147 - 0.8486i$	7

Table 5: Initial guesses and the computed resonances for $\delta = 0.2$.

$\tilde{k}_\ell$	k_ℓ	iteration numbers
$2.0462 - 0.2i$	$2.0139 - 0.2372i$	4
$4.5367 - 0.2372i$	$4.7283 - 0.6256i$	5
$8.9326 - 0.6256i$	$7.6572 - 0.9200i$	8
$12.0765 - 0.9200i$	$10.5837 - 1.3232i$	10
$15.2274 - 1.3232i$	$13.522 - 1.5703i$	10

Table 6: Computed resonances with refined meshes. $\delta = 0.02$.

$n_1 = 10\ n_2 = 40$	$n_1 = 20\ n_2 = 80$	$n_1 = 40\ n_2 = 160$	$n_1 = 60\ n_2 = 200$
$0.7656 - 0.0499i$	$0.7832 - 0.0479i$	$0.7691 - 0.0440i$	$0.7696 - 0.0436i$
$2.7379 - 0.1755i$	$2.7513 - 0.1642i$	$2.7390 - 0.1648i$	$2.7404 - 0.1638i$
$5.2698 - 0.1966i$	$5.2983 - 0.1847i$	$5.2933 - 0.1966i$	$5.2932 - 0.1958i$
$7.9744 - 0.3229i$	$8.0485 - 0.3196i$	$8.0414 - 0.3371i$	$8.0422 - 0.3337i$
$10.6749 - 0.2643i$	$10.8462 - 0.3399i$	$10.9015 - 0.3215i$	$10.9017 - 0.3234i$
$13.3940 - 0.3369i$	$13.8351 - 0.4129i$	$13.9003 - 0.4664i$	$13.8975 - 0.4619i$

Table 7: Computed resonances with refined meshes. $\delta = 0.1$.

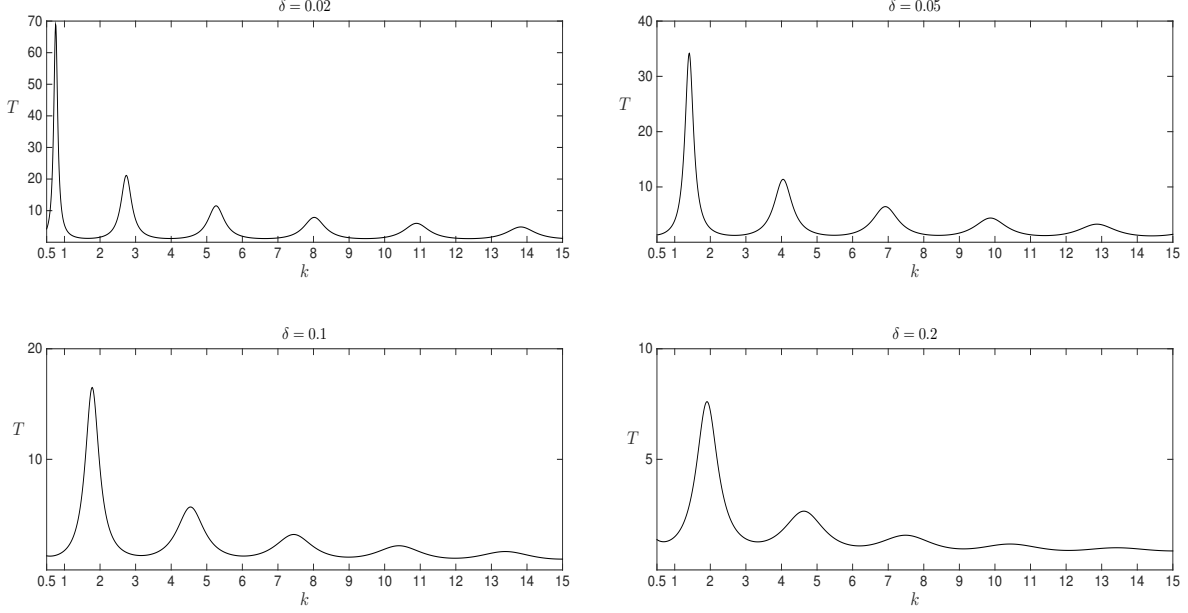| $n_1 = 10\ n_2 = 40$	$n_1 = 20\ n_2 = 80$	$n_1 = 40\ n_2 = 160$	$n_1 = 60\ n_2 = 200$
$1.8473 - 0.1246i$	$1.8501 - 0.1311i$	$1.8513 - 0.1318i$	$1.8513 - 0.1317i$
$4.6374 - 0.3645i$	$4.5851 - 0.3882i$	$4.5846 - 0.4188i$	$4.5856 - 0.4166i$
$7.5726 - 0.6238i$	$7.5187 - 0.5136i$	$7.5114 - 0.4881i$	$7.5106 - 0.4896i$
$10.5410 - 0.6004i$	$10.4920 - 0.7154i$	$10.5743 - 0.7727i$	$10.5698 - 0.7681i$
$13.5452 - 0.8596i$	$13.5147 - 0.8486i$	$13.4566 - 0.8557i$	$13.4609 - 0.8603i$

Figure 8: The transmittance T over the frequency band $[0.5, 15]$ for various slit sizes.

Example 3 We set the permittivity for the metal as $\varepsilon_m = -20 + 2i$ in the example. Again, $n_1 = 20$ and $n_2 = 80$ are used for discretizing the integrals over the horizontal and vertical slit boundaries respectively, and the tolerance for the Newton solver is 10^{-4}.

We compute the resonances for the slit size $\delta = 0.02$, 0.05, 0.1, and 0.2, respectively. The initial guesses for the resonances are shown in the first column of Tables 8 - 11 for various slit sizes. It is seen that they also provide good approximations of true resonances. Starting from these initial-guess values, the Newton method converges and the computed resonances are shown in the second column of Tables 8 - 11. The corresponding iteration numbers are given in the third columns, which demonstrate the robustness and the efficiency of the proposed computational approach.

For a given δ, it is observed from Figure 9 that the peaks for trasmittance T are consistent with the locations of the computed resonances, which confirms the accuracy of the integral equation method. Finally, for each δ, by noting that each peak in Figure 9 corresponds to one resonance in Table 8 - 11, we see that all resonances in the above frequency band that lie in the vicinity of the real axis are successfully solved. This again reflects the robustness of the proposed numerical method.

Table 8: Initial guesses and the computed resonances for $\delta = 0.02$.

$\tilde{k}_\ell$	k_ℓ	iteration numbers
$1.0514 - 0.02i$	$0.9064 - 0.3279i$	6
$2.701 - 0.3279i$	$2.6780 - 0.1963i$	6
$4.7417 - 0.3279i$	$4.8147 - 0.4001i$	7
$7.0393 - 0.4001i$	$7.1860 - 0.2835i$	6
$9.5072 - 0.4001i$	$9.8259 - 0.4966i$	9
$12.0915 - 0.4966i$	$12.3633 - 0.3438i$	9

Table 9: Initial guesses and the computed resonances for $\delta = 0.05$.

$\tilde{k}_\ell$	k_ℓ	iteration numbers
$0.7125 - 0.05i$	$0.5880 - 0.06154i$	8
$2.6093 - 0.0616i$	$2.6430 - 0.3223i$	12
$5.0005 - 0.3222i$	$5.1897 - 0.1900i$	7
$7.5861 - 0.3222i$	$8.0308 - 0.4645i$	14
$10.2648 - 0.4645i$	$10.7828 - 0.2818i$	14
$12.9943 - 0.4645i$	$13.9094 - 0.5254i$	20

Table 10: Initial guesses and the computed resonances for $\delta = 0.1$.

$\tilde{k}_\ell$	k_ℓ	iteration numbers
$1.1923 - 0.1i$	$1.1517 - 0.0627i$	6
$3.504 - 0.0626i$	$3.7293 - 0.4508i$	11
$6.0496 - 0.4508i$	$6.4636 - 0.2497i$	7
$10.383 - 0.4508i$	$9.5812 - 0.6125i$	11
$13.4649 - 0.6125i$	$12.2692 - 0.4306i$	17

Table 11: Initial guesses and the computed resonances for $\delta = 0.2$.

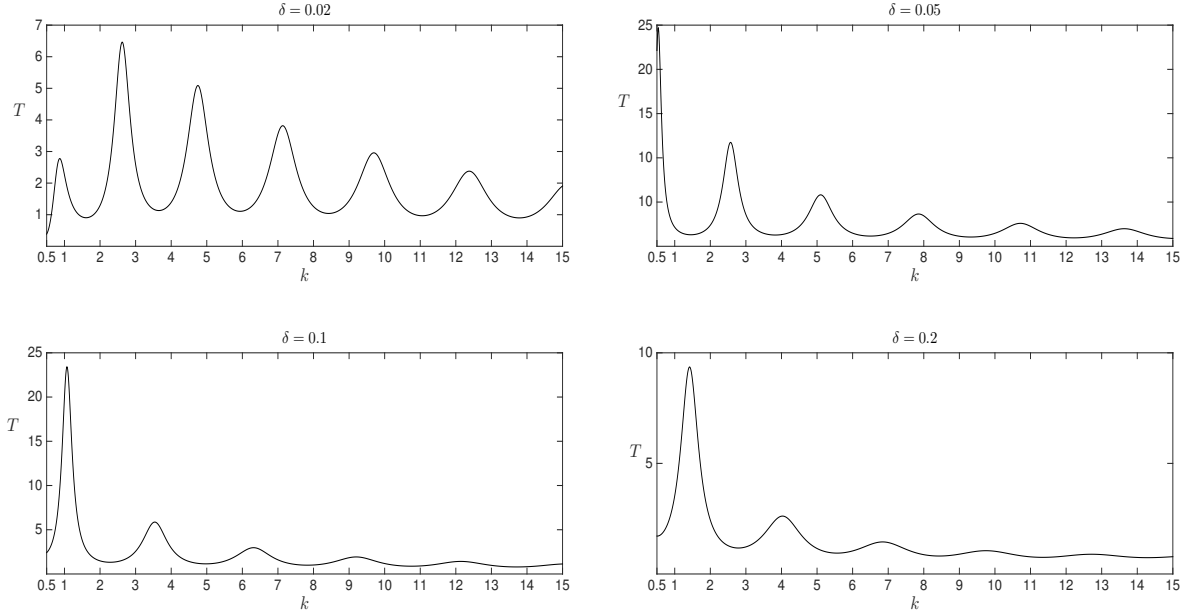| $\tilde{k}_\ell$	k_ℓ	iteration numbers
$1.5878 - 0.2i$	$1.5658 - 0.1011i$	8
$3.9938 - 0.1012i$	$4.4712 - 0.6928i$	9
$8.2869 - 0.6928i$	$7.119 - 0.4686i$	7
$11.4062 - 0.6928i$	$10.4770 - 1.0821i$	11
$14.5419 - 1.0821i$	$13.343 - 2.0182i$	11

Figure 9: The transmittance T over the frequency band $[0.5, 15]$ for various slit sizes.

6 Computation of resonances for the PEC slit

In this section, we discuss briefly the computational framework when the permittivity $|\varepsilon_m| \to \infty$ such that the metallic slab becomes a perfect conductor. This yields zero Neumann boundary condition along horizontal and vertical the metal-vacuum interfaces. In particular, the system of integral equations (2.25) is reduced to the ones formulated over the slit apertures Γ_1 and Γ_2 only, by observing that the contribution from the slit walls Γ_3 and Γ_4 vanishes as $|\varepsilon_m| \to \infty$. Alternatively, the perfect conductor model can be viewed as the limiting case for the approximate scattering model (4.1) such that $\partial_\nu \tilde{u} = 0$ on Γ_3 and Γ_4. This also leads to the system of integral equations (4.11) defined on the slit apertures, where the interior Green's function $g^i(x, y)$ is now given by the Green's function $G^s(x, y)$ for the slit geometry defined in (2.5). The scattering resonances are computed by solving the homogeneous problem corresponding to (4.11) and with $g^i(x, y) = G^s(x, y)$. We apply the Newton's method to solve the eigenvalue problem, where the asymptotic expansions of the resonances for the case of $\delta \ll 1$ are used as initial guesses. Such asymptotic expansions have been derived in [17]. We state the result in the following and refer to Theorem 4.4 in [17] for details.

Theorem 6.1 *If $\delta \ll 1$, the resonances of the scattering problem (1.1) when $|\varepsilon_m| = \infty$ are given by*

$$k_\ell = \ell\pi + 2\ell \cdot \delta \ln \delta + C_\ell \cdot \delta + O(\delta^2 \ln^2 \delta)$$

for $\ell\delta \ll 1$, where C_ℓ is a complex constant independent of δ and attains negative imaginary part.

We apply the integral equation method to compute the resonances when the slit size $\delta = 0.02, 0.05, 0.1$, and 0.2, respectively. To discretize the single-layer integral operators in (4.11), we set the number of grid points as $n_1 = 40$, and the tolerance for the Newton solver as 10^{-4}.

The strategy for choosing initial guesses $\{\tilde{k}_\ell\}_{\ell=1}^L$ is similar to that of the real metal case in Section 4, except that the complex-valued $O(\delta)$-term is now given explicitly for the PEC slit. As such we use the first three terms in the asymptotic expansion for the initial guess $\tilde{k}_1$. The obtained initial-guess values $\{\tilde{k}_\ell\}_{\ell=1}^L$, which are good approximations of true resonances, are shown in the first column of Tables 12 - 15 for various slit sizes. The second column of Tables 12 - 15 are the computed resonances $\{k_\ell\}_{\ell=1}^L$ obtained by solving the homogeneous equations (4.11) and starting from the initial-guess values. The corresponding iteration numbers are given in the third columns, which demonstrate the efficiency of the integral equation method. For fixed δ, each peak of the trasmittance T in Figure 10 corresponds to one resonance in Table 12 - 15, and the frequencies of the peaks are consistent with the locations of the computed resonances. Therefore, we see that all resonances in the above frequency band that lie in the vicinity of the real axis are solved accurately.

Table 12: Initial guesses and the computed resonances for $\delta = 0.02$.

$\tilde{k}_\ell$	k_ℓ	iteration numbers
$2.9682 - 0.0628i$	$2.9745 - 0.0567i$	2
$5.9702 - 0.0567i$	$6.000 - 0.1139i$	3
$8.9553 - 0.1139i$	$9.0463 - 0.1700i$	3
$11.9404 - 0.1670i$	$12.1052 - 0.2246i$	4

Table 13: Initial guesses and the computed resonances for $\delta = 0.05$.

$\tilde{k}_\ell$	k_ℓ	iteration numbers
$2.7998 - 0.1571i$	$2.8203 - 0.1275i$	3
$5.6840 - 0.1275i$	$5.7599 - 0.2558i$	4
$8.5261 - 0.2558i$	$8.7460 - 0.3769i$	4
$11.3681 - 0.3769i$	$11.7601 - 0.4902i$	5
$14.2101 - 0.4902i$	$14.7934 - 0.5964i$	5

Table 14: Initial guesses and the computed resonances for $\delta = 0.1$.

$\tilde{k}_\ell$	k_ℓ	iteration numbers
$2.5965 - 0.3142i$	$2.6378 - 0.2227i$	4
$5.3622 - 0.2227i$	$5.4910 - 0.4451i$	4
$8.0432 - 0.4451i$	$8.4239 - 0.6463i$	5
$10.7243 - 0.6463i$	$11.4005 - 0.8291i$	6
$13.4054 - 0.8291i$	$14.4046 - 0.9982i$	7

Table 15: Initial guesses and the computed resonances for $\delta = 0.2$.

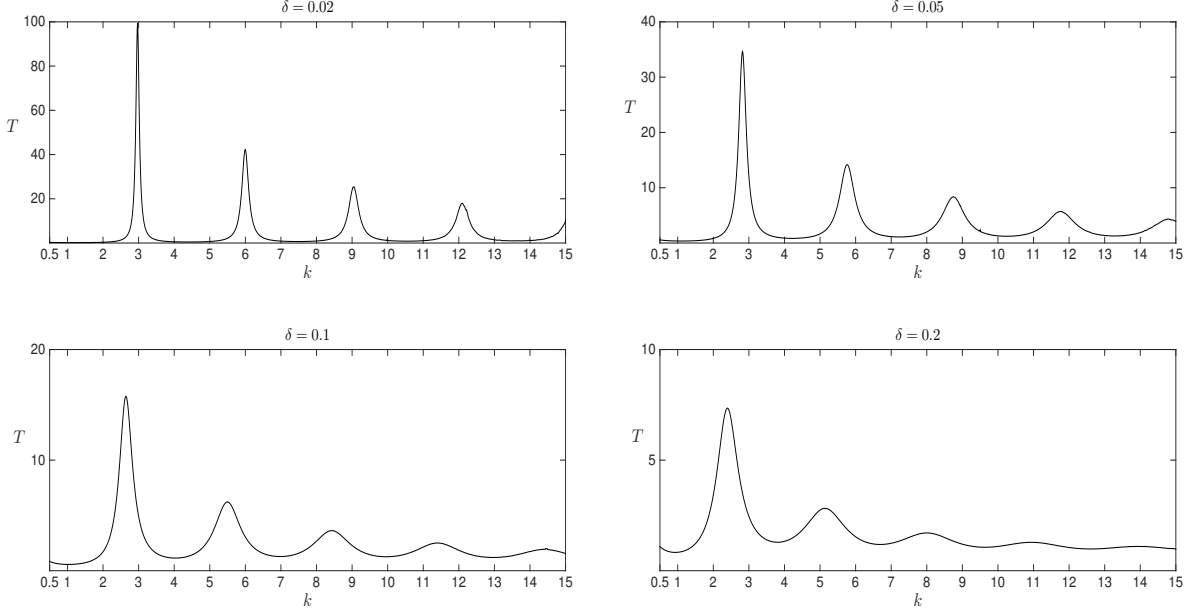| $\tilde{k}_\ell$	k_ℓ	iteration numbers
$2.3286 - 0.6283i$	$2.3838 - 0.3635i$	5
$4.9956 - 0.3635i$	$5.1314 - 0.7273i$	5
$7.4935 - 0.7273i$	$8.0008 - 1.0477i$	6
$9.9913 - 1.0477i$	$10.9308 - 1.3435i$	7
$12.4891 - 1.3435i$	$13.9010 - 1.6311i$	9

Figure 10: The transmittance T over the frequency band $[0.5, 15]$ for various slit sizes.

Acknowledgements

Appendix A   Green's functions in the layered medium

We derive explicitly the Green's function when $y \in \Omega_1$. Taking the Fourier transform of (2.1) with respect to the variable $x_1 - y_1$, the Green's function in the Fourier domain satisfies

$$\hat{G}_1''(\xi; x_2, y_2) + (k^2 \varepsilon(x_2) - \xi^2)\hat{G}_1(\xi; x_2, y_2) = \tilde{\delta}(x_2 - y_2), \quad -\infty < x_2 < \infty,$$

$$[\hat{G}_1(\xi; x_2, y_2)] = \left[\frac{1}{\varepsilon}\hat{G}_1'(\xi; x_2, y_2)\right] = 0 \quad x_2 = 0, x_2 = 1.$$

Let

$$\rho_0(\xi) = \sqrt{k^2 - \xi^2}, \quad \rho_m(\xi) = \sqrt{k^2 \varepsilon_m - \xi^2},$$

$$p(\xi) = (\varepsilon_m + 1)\left(\rho_0^2(\xi)\varepsilon_m^2 - \rho_m^2(\xi)\right) - (\varepsilon_m - 1)\left(\rho_0(\xi)\varepsilon_m - \rho_m(\xi)\right)^2,$$

$$q(\xi) = \left(\rho_0(\xi)\varepsilon_m - \rho_m(\xi)\right)^2 e^{i2\rho_m} - \left(\rho_0(\xi)\varepsilon_m + \rho_m(\xi)\right)^2.$$

37

Then the solution

$$
\hat{G}_1(\xi; x_2, y_2) = \begin{cases}
\dfrac{1}{2i\rho_0}e^{i\rho_0|x_2-y_2|} + R\,e^{i\rho_0(x_2+y_2-2)} & x_2 > 1, \\[2mm]
T_1\,e^{i\rho_0(y_2-1)}e^{i\rho_m(1+x_2)} + T_2\,e^{i\rho_0(y_2-1)}e^{i\rho_m(1-x_2)} & 0 < x_2 < 1, \\[2mm]
T_3\,e^{i\rho_0(y_2-x_2-1)} & x_2 < 0,
\end{cases}
$$

where the coefficients

$$
R = \frac{1}{2i\rho_0 q}\cdot\left(\rho_0^2\varepsilon_m^2 - \rho_m^2\right)\left(e^{i2\rho_m}-1\right), \quad T_1 = \frac{i}{q}\cdot\varepsilon_m(\rho_m - \rho_0\varepsilon_m)
$$

$$
T_2 = \frac{i}{q}\cdot\varepsilon_m(\rho_m + \rho_0\varepsilon_m), \quad T_3 = \frac{2i}{q}\cdot\varepsilon_m\rho_m e^{i\rho_m}.
$$

We decompose the coefficient R as $R := R_0 + R_1$, where

$$
R_0 = \frac{\varepsilon_m - 1}{\varepsilon_m + 1}\cdot\frac{1}{2i\rho_0} \quad\text{and}\quad R_1 = \frac{k^2\varepsilon_m(\varepsilon_m-1)}{i(\varepsilon_m+1)}\cdot\frac{\rho_0\varepsilon_m + \rho_m}{\rho_0\left(\rho_o + \rho_m\right)q} + \frac{1}{2i(\varepsilon_m+1)}\cdot\frac{pe^{i2\rho_m}}{\rho_0 q}. \tag{A.1}
$$

For $0 < x_2 < 1$, we split $\hat{G}_1(\xi; x_2, y_2)$ as

$$
\frac{\varepsilon_m}{\varepsilon_m+1}\cdot\frac{1}{i\rho_0}e^{i\rho_0(y_2-x_2)} + \left[T_1\,e^{i\rho_0(y_2-1)}e^{i\rho_m(1+x_2)} + T_2\,e^{i\rho_0(y_2-1)}e^{i\rho_m(1-x_2)} - \frac{\varepsilon_m}{\varepsilon_m+1}\cdot\frac{1}{i\rho_0}e^{i\rho_0(y_2-x_2)}\right].
\tag{A.2}
$$

Apply the inverse Fourier transform for $\hat{G}_1(\xi; x_2, y_2)$ by using the decomposition (A.1), (A.2) and the identity

$$
\frac{1}{2\pi}\int_{-\infty}^{\infty}\frac{1}{2i\rho_0(\xi)}e^{i\rho_0(\xi)(x_2-y_2)}e^{i\xi(x_1-y_1)}d\xi = -\frac{i}{4}H_0^{(1)}(k|x-y|),
$$

we obtain

$$
G_1(x,y) = \begin{cases}
-\dfrac{i}{4}\left(H_0^{(1)}(k|x-y|) + \dfrac{\varepsilon_m-1}{\varepsilon_m+1}H_0^{(1)}(k|x'-y|)\right) + g_{11}(x,y), & x \in \Omega_1, \\[3mm]
-\dfrac{i\varepsilon_m}{2(\varepsilon_m+1)}H_0^{(1)}(k|x-y|) + g_{12}(x,y)), & x \in \Omega_2, \\[3mm]
g_{13}(x,y), & x \in \Omega_3,
\end{cases}
$$

where x' is the reflection of x by $x_2 = 1$. The functions g_{1j} $(j = 1, 2, 3)$ are the Sommerfeld integrals given by

$$
\begin{aligned}
g_{11}(x,y) &= \frac{1}{2\pi}\int_{-\infty}^{\infty}R_1(\xi)e^{i\rho_0(x_2+y_2-2)}e^{i\xi(x_1-y_1)}\,d\xi \\[2mm]
&= \frac{k^2\varepsilon_m(\varepsilon_m-1)}{i\pi(\varepsilon_m+1)}\int_0^{\infty}\frac{\rho_0(\xi)\varepsilon_m + \rho_m(\xi)}{\rho_0(\xi)\left(\rho_0(\xi)+\rho_m(\xi)\right)q(\xi)}e^{i\rho_0(\xi)(x_2+y_2-2)}\cos(\xi(x_1-y_1))\,d\xi \\[2mm]
&\quad + \frac{1}{2\pi i(\varepsilon_m+1)}\int_0^{\infty}\frac{p(\xi)e^{i2\rho_m(\xi)}}{\rho_0(\xi)q(\xi)}e^{i\rho_0(\xi)(x_2+y_2-2)}\cos(\xi(x_1-y_1))\,d\xi;
\end{aligned}
\tag{A.3}
$$

$$g_{12}(x, y) = \frac{1}{2\pi} \int_{-\infty}^{\infty} \left[T_1 \, e^{i\rho_0(y_2-1)} e^{i\rho_m(1+x_2)} + T_2 \, e^{i\rho_0(y_2-1)} e^{i\rho_m(1-x_2)} - \frac{\varepsilon_m}{\varepsilon_m + 1} \cdot \frac{1}{i\rho_0} e^{i\rho_0(y_2-x_2)} \right] e^{i\xi(x_1-y_1)} \, d\xi$$

$$= \frac{i\varepsilon_m}{\pi} \int_0^{\infty} \frac{\rho_m(\xi) - \rho_0(\xi)\varepsilon_m}{q(\xi)} \, e^{i\rho_0(\xi)(y_2-1)} e^{i\rho_m(\xi)(1+x_2)} \cos(\xi(x_1 - y_1)) \, d\xi$$

$$+ \frac{i\varepsilon_m}{\pi} \int_0^{\infty} \left[\frac{\rho_m(\xi) + \rho_0(\xi)\varepsilon_m}{q(\xi)} \, e^{i\rho_0(\xi)(y_2-1)} e^{i\rho_m(\xi)(1-x_2)} \right.$$

$$\left. + \frac{1}{\varepsilon_m + 1} \cdot \frac{1}{\rho_0(\xi)} e^{i\rho_0(\xi)(y_2-x_2)} \right] \cos(\xi(x_1 - y_1)) \, d\xi \tag{A.4}$$

$$g_{13}(x, y) = \frac{1}{2\pi} \int_{-\infty}^{\infty} T_3 \, e^{i\rho_0(y_2-x_2-1)} e^{i\xi(x_1-y_1)} \, d\xi$$

$$= \frac{2i\varepsilon_m}{\pi} \int_0^{\infty} \frac{\rho_m(\xi)}{q(\xi)} e^{i\rho_m(\xi)} e^{i\rho_0(\xi)(y_2-x_2-1)} \cos(\xi(x_1 - y_1)) \, d\xi. \tag{A.5}$$

For $y \in \Omega_2$, by analogous derivations, it can be shown that

$$G_2(x, y) = \begin{cases} -\dfrac{i}{2} \dfrac{1}{\varepsilon_m + 1} H_0^{(1)}(k_m|x - y|) + g_{21}(x, y), & x \in \Omega_1, \\[2mm] -\dfrac{i}{4} \left(H_0^{(1)}(k_m|x - y|) + \dfrac{1 - \varepsilon_m}{1 + \varepsilon_m} H_0^{(1)}(k_m|x' - y|) + \dfrac{1 - \varepsilon_m}{1 + \varepsilon_m} H_0^{(1)}(k_m|x'' - y|) \right) \\[2mm] + g_{22}(x, y), & x \in \Omega_2, \\[2mm] -\dfrac{i}{2} \dfrac{1}{\varepsilon_m + 1} H_0^{(1)}(k_m|x - y|) + g_{23}(x, y), & x \in \Omega_3, \end{cases}$$

where x' and x'' are the reflection of x by $x_2 = 1$ and $x_2 = 0$, respectively. The functions g_{2j} $(j = 1, 2, 3)$ are the Sommerfeld integrals given by

$$g_{21}(x, y) = \frac{i}{\pi} \int_0^{\infty} \frac{\rho_m(\xi) - \rho_0(\xi)\varepsilon_m}{q(\xi)} \, e^{i\rho_0(\xi)(x_2-1)} e^{i\rho_m(\xi)(1+y_2)} \cos(\xi(x_1 - y_1)) \, d\xi$$

$$+ \frac{i}{\pi} \int_0^{\infty} \left[\frac{\rho_m(\xi) + \rho_0(\xi)\varepsilon_m}{q(\xi)} \, e^{i\rho_0(\xi)(x_2-1)} e^{i\rho_m(\xi)(1-y_2)} \right.$$

$$\left. + \frac{1}{\varepsilon_m + 1} \cdot \frac{1}{\rho_m(\xi)} e^{i\rho_m(\xi)(x_2-y_2)} \right] \cos(\xi(x_1 - y_1)) \, d\xi; \tag{A.6}$$

$$g_{22}(x, y) = \frac{ik^2\varepsilon_m(\varepsilon_m - 1)}{\pi(\varepsilon_m + 1)} \int_0^{\infty} \frac{\rho_0(\xi)\varepsilon_m + \rho_m(\xi)}{\rho_m(\xi)\,(\rho_0(\xi) + \rho_m(\xi))\,q(\xi)} \left(e^{i\rho_0(\xi)(x_2+y_2)} + e^{i\rho_0(\xi)(2-x_2-y_2)} \right) \cos(\xi(x_1 - y_1)) \, d\xi$$

$$+ \frac{i}{2\pi} \int_0^{\infty} \frac{(\rho_0(\xi)\varepsilon_m - \rho_m(\xi))^2 e^{i2\rho_m}}{\rho_m(\xi)q(\xi)} \left(e^{i\rho_m(\xi)(x_2-y_2)} + e^{i\rho_m(\xi)(y_2-x_2)} \right) \cos(\xi(x_1 - y_1)) \, d\xi \tag{A.7}$$

$$- \frac{i(\varepsilon_m - 1)}{2\pi(\varepsilon_m + 1)} \int_0^{\infty} \frac{(\rho_0(\xi)\varepsilon_m - \rho_m(\xi))^2 e^{i2\rho_m}}{\rho_m(\xi)q(\xi)} \left(e^{i\rho_m(\xi)(x_2+y_2)} + e^{i\rho_m(\xi)(2-x_2-y_2)} \right) \cos(\xi(x_1 - y_1)) \, d\xi;$$

$$g_{23}(x,y) = \frac{i}{\pi} \int_0^\infty \frac{\rho_m(\xi) - \rho_0(\xi)\varepsilon_m}{q(\xi)} e^{-i\rho_0(\xi)x_2} e^{i\rho_m(\xi)(2-y_2)} \cos(\xi(x_1 - y_1)) \, d\xi$$

$$+ \frac{i}{\pi} \int_0^\infty \left[\frac{\rho_m(\xi) + \rho_0(\xi)\varepsilon_m}{q(\xi)} e^{-i\rho_0(\xi)x_2} e^{i\rho_m(\xi)y_2} \right.$$

$$\left. + \frac{1}{\varepsilon_m + 1} \cdot \frac{1}{\rho_m(\xi)} e^{\rho_m(\xi)(x_2 - y_2)} \right] \cos(\xi(x_1 - y_1)) \, d\xi. \tag{A.8}$$

Appendix B   Derivations of (2.16)

Let $\Gamma_t := \{x_2 = 1\}$ and $\Gamma_b := \{x_2 = 0\}$ be the top and bottom of the metallic slab respectively. For $y \in \Omega_1$, we apply the Green's second identity in the domain Ω_1 and Ω_3 to obtain

$$u^s(y) = \int_{\Gamma_t} G_1(x,y) \frac{\partial u^s(x)}{\partial \nu_x} - \frac{\partial G_1(x,y)}{\partial \nu_x} u^s(x) \, ds_x. \tag{B.1}$$

$$0 = \int_{\Gamma_b} G_1(x,y) \frac{\partial u^s(x)}{\partial \nu_x} - \frac{\partial G_1(x,y)}{\partial \nu_x} u^s(x) \, ds_x, \tag{B.2}$$

where ν is the unit normal pointing to the domains Ω_1 and Ω_2. Applying the Green's second identity in the domain Ω_δ^- and Ω_δ^+ respectively, we have

$$0 = \int_{\Gamma_t^- \cup \Gamma_b^-} \frac{\partial G_1(x,y)}{\partial \nu_x} u^s(x) - G_1(x,y) \frac{\partial u^s(x)}{\partial \nu_x} \, ds_x + \int_{\Gamma_3} G_1(x,y) \frac{\partial u^s(x)}{\partial \nu_x} - \frac{\partial G_1(x,y)}{\partial \nu_x} u^s(x) \, ds_x,$$
$$\tag{B.3}$$

$$0 = \int_{\Gamma_t^+ \cup \Gamma_b^+} \frac{\partial G_1(x,y)}{\partial \nu_x} u^s(x) - G_1(x,y) \frac{\partial u^s(x)}{\partial \nu_x} \, ds_x + \int_{\Gamma_4} G_1(x,y) \frac{\partial u^s(x)}{\partial \nu_x} - \frac{\partial G_1(x,y)}{\partial \nu_x} u^s(x) \, ds_x.$$
$$\tag{B.4}$$

In the above, the line segments

$$\Gamma_t^- := \{x \in \Gamma_t \,|\, x_1 < 0\}, \quad \Gamma_t^+ := \{x \in \Gamma_t \,|\, x_1 > \delta\},$$
$$\Gamma_b^- := \{x \in \Gamma_b \,|\, x_1 < 0\}, \quad \Gamma_b^+ := \{x \in \Gamma_b \,|\, x_1 > \delta\}.$$

Taking the sum (B.1) + (B.2) + $\dfrac{1}{\varepsilon_m} \times \big((\text{B.3}) + (\text{B.4})\big)$ and using the continuity conditions for u^s and G_1 along the metal-vacuum interfaces, it follows that

$$u^s(y) = \sum_{j=1}^4 \int_{\Gamma_j} G_1(x,y) \left(\gamma_j \frac{\partial u^s(x)}{\partial \nu_x} \right) - \left(\gamma_j \frac{\partial G_1(x,y)}{\partial \nu_x} \right) u^s(x) \, ds_x.$$

The formula can be obtained similarly for $y \in \Omega_2$, Ω_δ^- and Ω_δ^+ respectively.

Appendix C Eigenvalues and eigenmodes for the operator $\mathcal{L}_n$

The operator $\mathcal{L}_n$ is defined as

$$\mathcal{L}_n v := \left(\frac{1}{\tilde{\varepsilon}(x_1)} v'(x_1) \right)' + \left(k^2 - \frac{(n\pi)^2}{\tilde{\varepsilon}(x_1)} \right) v(x_1), \quad -\infty < x_1 < \infty,$$

where the permittivity $\tilde{\varepsilon}(x_1) = 1$ for $x_1 \in (0, \delta)$ and $\tilde{\varepsilon}(x_1) = \varepsilon'_m$ for $x_1 \neq [0, \delta]$. We solve the eigenvalue problem $\mathcal{L}_n v = -\lambda v$. To this end, we express the solution as

$$v(x_1) = \begin{cases} c_1 e^{\zeta_n x_1} & x_1 < 0, \\ c_3 e^{i\alpha_n x_1} + c_4 e^{-i\alpha_n x_1} & 0 < x_1 < \delta, \\ c_2 e^{\zeta_n(\delta - x_1)} & x_1 > \delta, \end{cases}$$

where $\zeta_n(\lambda) = \sqrt{(n\pi)^2 - \varepsilon'_m \lambda}$, $\alpha_n(\lambda) = \sqrt{\lambda - (n\pi)^2}$. Imposing the continuity conditions leads to a linear system for the coefficients c_1, c_2, c_3 and c_4, and the condition for the existence of non-trivial solution v is given by

$$e^{i\alpha_n(\lambda)\delta} = \pm \frac{\zeta_n(\lambda) - i\alpha_n(\lambda)\varepsilon'_m}{\zeta_n(\lambda) + i\alpha_n(\lambda)\varepsilon'_m}.$$

We restrict the discussion for $\lambda \in ((n\pi)^2, +\infty)$. Then the above nonlinear equation leads to

$$\alpha_n \delta - p\pi = \arg \frac{\zeta_n - i\alpha_n \varepsilon'_m}{\zeta_n + i\alpha_n \varepsilon'_m}, \quad p = 0, 1, 2, 3, \cdots$$

If $|\varepsilon'_m| \gg 1$, then the coefficient α_n is given by

$$\alpha_{np}\delta \approx p\pi + \theta_0 \approx (p+1)\pi, \quad \text{where } \theta_0 = 2 \arctan \sqrt{|\varepsilon'_m|} \approx \pi. \tag{C.1}$$

Correspondingly, the eigenvalues

$$\lambda = \lambda_{np} \approx (n\pi)^2 + \left(\frac{p\pi + \theta_0}{\delta} \right)^2 \quad \text{and} \quad \zeta_{np} = \sqrt{(n\pi)^2 - \varepsilon'_m \lambda_{np}}, \quad p = 0, 1, 2, 3, \cdots. \tag{C.2}$$

The eigenmodes are

$$v_{np}(x) = \begin{cases} c_{np}(1 + e^{i\alpha_{np}\delta})e^{\zeta_{np}x_1}, & x_1 < 0, \\ c_{np}(e^{i\alpha_{np}x_1} + e^{-i\alpha_{np}(\delta - x_1)}), & 0 < x_1 < \delta, \\ c_{np}(1 + e^{i\alpha_{np}\delta})e^{\zeta_{np}(\delta - x_1)}, & x_1 > \delta, \end{cases}$$

and

$$v_{np}(x) = \begin{cases} c_{np}(1 - e^{i\alpha_{np}\delta})e^{\zeta_{np}x_1}, & x_1 < 0, \\ c_{np}(e^{i\alpha_{np}x_1} - e^{-i\alpha_{np}(\delta - x_1)}), & 0 < x_1 < \delta, \\ -c_{np}(1 - e^{i\alpha_{np}\delta})e^{\zeta_{np}(\delta - x_1)}, & x_1 > \delta, \end{cases}$$

for odd and even p respectively, where the constants c_{np} are normalization constants such that $||v_{np}||_{L^2(-\infty,\infty)} = 1$. Recall that α_{np} and ζ_{np} are given by (C.1) and (C.2). By carrying out standard asymptotic analysis, we have the following lemma:

Lemma C.1 *Let $\delta \ll 1$ and $|\varepsilon'_m| \sim O(1/\delta)$, then the following holds:*

$$v_{np}(x_1) = \sqrt{\frac{2}{\delta}} \left(\cos\left(\frac{(p+1)\pi x_1}{\delta} \right) + O(\delta^s) \right), s \geq 1/2, \quad for\ x_1 \in (0, \delta),$$

$$v_{np}(x_1) \sim O\left(e^{-r\sqrt{|\varepsilon'_m|/\delta}} \right) \quad for\ x_1 \neq [0, \delta],$$

where r is the distance of x_1 from the interval $(0, \delta)$.

References

[1] F. J. GARCÍA DE ABAJO, *Colloquium: Light scattering by particle and hole arrays*, Rev. Mod. Phy., **79** (2007), 1267.

[2] R. ADAMS AND J. FOURNIER, *Sobolev Spaces*, vol. 140, Academic Press, 2003.

[3] H. AMMARI, P. MILLIEN, M. RUIZ, AND H. ZHANG, *Mathematical analysis of plasmonic nanoparticles: the scalar case. Arch. Ration. Mech. An.*, **224** (2017), 597-658.

[4] H. AMMARI AND H. ZHANG, *A mathematical theory of super-resolution by using a system of sub-wavelength Helmholtz resonators*, Comm. Math. Phys., **337** (2015), 379-428.

[5] H. AMMARI, B. FITZPATRICK, D. GONTIER, H. LEE AND H. ZHANG, *Minnaert resonances for acoustic waves in bubbly media*, Annales de l'Institut Henri Poincaré: Analyse Nonlinéaire, to appear.

[6] E. BONNETIER AND F. TRIKI, *Asymptotic of the Green function for the diffraction by a perfectly conducting plane perturbed by a sub-wavelength rectangular cavity*, Math. Meth. Appl. Sci., **33** (2010), 772-798.

[7] J. F. BABADJIAN, E. BONNETIER AND F. TRIKI, *Enhancement of electromagnetic fields caused by interacting subwavelength cavities*, Multiscale Model. Simul., **8** (2010), 1383-1418.

[8] J. BOYD, *Exponentially convergent Fourier-Chebshev quadrature schemes on bounded and infinite intervals*, J. Sci. Comput., **2** (1987), 99-109.

[9] X. CHEN *et al*, *Atomic layer lithography of wafer-scale nanogap arrays for extreme confinement of electro-magnetic waves*, Nat. Commun., **4** (2013), 2361.

[10] D. COLTON AND R. KRESS, *Inverse Acoustic and Electromagnetic Scattering Theory*, Applied Mathematical Sciences, vol. 93, Springer-Verlag, Berlin, 1998.

[11] T. W. EBBESEN, H. J. LEZEC, H. F. GHAEMI, T. THIO, AND P. A. WOLFF, *Extraordinary optical transmission through sub-wavelength hole arrays*, Nature, **391** (1998), 667-669.

[12] F. J. GARCIA-VIDAL, L. MARTIN-MORENO, T. W. EBBESEN, AND L. KUIPERS, *Light passing through subwavelength apertures*, Rev. Modern Phys., **82** (2010), 729-787.

[13] I. GRADSHTEYN AND I. RYZHIK, Table of Integrals, Series, and Products. Academic Press, 2014.

[14] Z. HU, J. LIN, Y. Y. LU, AND S-H. OH, *Fast vertical mode expansion method for the simulation of extraordinary terahertz field enhancement in an annular nanogap*, J. Opt. Soc. Amer. B, **35** (2018), 30-38.

[15] J. LIN, S.-H. OH, H.-M. NGUYEN, AND F. REITICH, *Field enhancement and saturation of millimeter waves inside a metallic nanogap*, Opt. Express, **22** (2014), pp. 14402-14410.

[16] J. LIN AND F. REITICH, *Electromagnetic field enhancement in small gaps: a rigorous mathematical theory*, SIAM J. Appl. Math., **75** (2015), 2290-2310.

[17] J. LIN AND H. ZHANG, *Scattering and field enhancement of a perfect conducting narrow slit*, SIAM J. Appl. Math., (2017), 951-976.

[18] J. LIN AND H. ZHANG, *Scattering by a periodic array of subwavelength slits I: field enhancement in the diffraction regime*, Multiscale Model. Simul., 16 (2018), pp. 922-953.

[19] J. LIN AND H. ZHANG, *Scattering by a periodic array of subwavelength slits II: surface bound states, total transmission and field enhancement in the homogenization regimes*, Multiscale Model. Simul., 16 (2018), pp. 954-990.

[20] J. LIN AND H. ZHANG, *Mathematical theory for plasmonic resonances in a narrow metallic slit*, in preparation.

[21] X. LU, H. SHI, AND Y. Y. LU, *Vertical mode expansion method for transmission of light through a single circular hole in a slab*, J. Opt. Soc. Am. A, **31** (2014), 293-300.

[22] X. LU AND Y. Y. LU, *Analyzing bull's eye structures by a vertical mode expansion method with rotational symmetry*, J. Opt. Soc. Amer. B, **32** (2015), 2294-2298.

[23] R. KRESS, *A Nystrom method for boundary integral equations in domains with corners*, Numer. Math., **58** (1990), 145-161.

[24] V. MEHRMANN AND H. VOSS, *Nonlinear eigenvalue problems: A challenge for modern eigenvalue methods*, GAMM-Mitteilungen, **27** (2004), 121-152.

[25] N. NICOROVICI, R. MCPHEDRAN, AND R. PETIT, *Efficient calculation of the Green?s function for electromagnetic scattering by gratings*, Phy. Rev. E, **49** (1994), 4563.

[26] M. A. ORDAL, *et al*, *Optical properties of the metals Al, Co, Cu, Au, Fe, Pb, Ni, Pd, Pt, Ag, Ti and W in the infrared and far infrared*, Appl. Opt., **22** (1983), 1099-1119

[27] M. PAULUS, P. GAY-BALMAZ, AND O. MARTIN, *Accurate and efficient computation of the Green's tensor for stratified media*, Phy. Rev. E, **62** (2000), 5797.

[28] C. PEREZ-ARANCIBIA AND O. BRUNO, *High-order integral equation methods for problems of scattering by bumps and cavities on half-planes*, J. Opt. Soc. Amer. A, **31** (2014), 1738-1746.

[29] A. RUHE, *Algorithms for the nonlinear eigenvalue problem*, SIAM J. Numer. Anal., **10** (1973), 674-689.

[30] S. RODRIGO, F. LEON-PEREZ, AND L. MARTIN-MORENO, *Extraordinary optical transmission: fundamentals and applications*, Proceedings of the IEEE, **104** (2016) 2288-2306.